

Article

Modeling Typhoid Fever Dynamics: Stability Analysis and Periodic Solutions in Epidemic Model with Partial Susceptibility

Fawaz K. Alalhareth ^{1,†} , Mohammed H. Alharbi ^{2,†}  and Mahmoud A. Ibrahim ^{3,4,*,†} 

- ¹ Department of Mathematics, College of Arts & Sciences, Najran University, Najran, Saudi Arabia
² Department of Mathematics, College of Science, University of Jeddah, Jeddah 21589, Saudi Arabia; mhhharbi1@uj.edu.sa
³ Bolyai Institute, University of Szeged, Aradi vértanúk tere 1., 6720 Szeged, Hungary
⁴ Department of Mathematics, Faculty of Science, Mansoura University, Mansoura 35516, Egypt
* mibrahim@math.u-szeged.hu or mahmoud_ali@mans.edu.eg
† These authors contributed equally to this work.

Abstract: Mathematical models play a crucial role in predicting disease dynamics and estimating key quantities. Non-autonomous models offer the advantage of capturing temporal variations and changes in the system. In this study, we analyzed the transmission of typhoid fever in a population using a compartmental model that accounted for dynamic changes occurring periodically in the environment. First, we determined the basic reproduction number, \mathcal{R}_0 , for the periodic model and derived the time-average reproduction rate, $[\mathcal{R}_0]$, for the non-autonomous model as well as the basic reproduction number, \mathcal{R}_0^A , for the autonomous model. We conducted an analysis to examine the global stability of the disease-free solution and endemic periodic solutions. Our findings demonstrated that when $\mathcal{R}_0 < 1$, the disease-free solution was globally asymptotically stable, indicating the extinction of typhoid fever. Conversely, when $\mathcal{R}_0 > 1$, the disease became endemic in the population, confirming the existence of positive periodic solutions. We also presented numerical simulations that supported these theoretical results. Furthermore, we conducted a sensitivity analysis of \mathcal{R}_0^A , $[\mathcal{R}_0]$ and the infected compartments, aiming to assess the impact of model parameters on these quantities. Our results showed that the human-to-human infection rate has a significant impact on the reproduction number, while the environment-to-human infection rate and the bacteria excretion rate affect long-cycle infections. Moreover, we examined the effects of parameter modifications and how they impact the implementing of efficient control strategies to combat TyF. Although our model is limited by the lack of precise parameter values, the qualitative results remain consistent even with alternative parameter settings.

Keywords: typhoid fever; seasonal model; partially susceptible; reproduction numbers; global stability; periodic solutions; sensitivity analysis

MSC: 34A99; 34C25; 34C60; 92D30



Citation: Alalhareth, F.K.; Alharbi, M.H.; Ibrahim, M.A. Modeling Typhoid Fever Dynamics: Stability Analysis and Periodic Solutions in Epidemic Model with Partial Susceptibility. *Mathematics* **2023**, *11*, 3713. <https://doi.org/10.3390/math11173713>

Academic Editor: Gonzalo Robledo

Received: 5 July 2023

Revised: 22 August 2023

Accepted: 27 August 2023

Published: 29 August 2023



Copyright: © 2023 by the authors. Licensee MDPI, Basel, Switzerland. This article is an open access article distributed under the terms and conditions of the Creative Commons Attribution (CC BY) license (<https://creativecommons.org/licenses/by/4.0/>).

1. Introduction

Typhoid fever (TyF), caused by the bacteria *Salmonella Typhi*, is a highly infectious illness. TyF is a leading cause of disease and death in regions with few medical facilities. Food and water contamination, lack of sanitation, and intimate personal contact between infected people are the most common ways that the disease is spread [1,2]. High fever that persists, headache, weakness, stomach discomfort, and either constipation or diarrhea are all signs of typhoid. Some individuals may develop a skin rash, and in the most extreme situations, typhoid may be deadly [3]. TyF has a significant worldwide impact, especially in low- and middle-income nations where sanitary infrastructure is weak and safe drinking

water is scarce. The World Health Organization (WHO) reports that roughly 110,000 people die from TyF each year out of an estimated 9 million annual infections. In many third-world nations, particularly those with inadequate sanitation and few supplies of potable water, the disease is prevalent. Examples of such areas include South Asia, India, Pakistan, and Bangladesh, which are particularly affected [3–5]. The liver, spleen, digestive tract, and bone marrow are only a few of the organs susceptible to damage from TyF. The gallbladder of chronic typhoid carriers may function as a reservoir for the germs due to the formation of a bio-film. This can lead to intermittent shedding of bacteria into the stool, potentially transmitting the disease to others [6,7]. Recovery from TyF can lead to partial immunity, reducing the risk of re-infection or milder symptoms. The immune system produces antibodies during the first infection, which recognize and combat future infections. However, partial immunity does not guarantee complete protection and may not work against other *Salmonella* strains [8,9].

Mathematical models are employed to demonstrate the dynamics of infectious diseases (e.g., [10–15]). Several mathematical models focusing on TyF dynamics have considered that transmission occurs only via direct contact between infected and susceptible persons [12,16]. Alternatively, some models have assumed that the disease is transmitted only through environmental factors like contaminated food and water [10,11]. In contrast, other models have included direct and environmental transmission dynamics [17,18]. Most of these models are autonomous models, where the model's parameters are constant and do not require external input to describe their behavior over time. For instance, Irena and Gakkhar [19] studied a two-strain mathematical model analyzing antimicrobial-resistant typhoid infection revealing that transmission rates and bacterial consumption affect \mathcal{R}_0 (basic reproduction number). The development of resistance due to treatment does not have an impact \mathcal{R}_0 . However, it does contribute to the elevated presence of resistant strains in a state of co-existence equilibrium. To mitigate the transmission of antimicrobial-resistant *Salmonella* Typhi strains, the study recommends promoting access to clean and potable water and practicing appropriate sanitation methods. Abboubakar and Racke [20] studied a compartmental model for preventing TyF, considering control mechanisms like an imperfect vaccine, hygiene practices, and therapeutic measures. Clinical data from Mbandjock, Cameroon, demonstrated the need for a comprehensive approach involving large-scale immunization, environmental sanitation, and appropriate therapeutic interventions to effectively control TyF. Pitzer et al. [18] modeled an autonomous system, dividing the population into two populations depending on their susceptibility (fully and partially susceptible). The evaluation conducted in the study examines both the direct and indirect impacts of typhoid vaccination. The findings indicate that vaccination can provide immediate indirect protection and contribute to a reduction in typhoid cases in the short term. However, relying solely on vaccination is improbable to lead to the complete elimination of the disease. The extent of indirect protection achieved through vaccination is influenced by assumptions made about chronic carriers of the infection.

Furthermore, some models (e.g., [21,22]) are non-autonomous models where some of the model's parameters are time-dependent parameters. In a study on TyF transmission dynamics [21], a system of non-linear differential equations is formulated with a time-dependent infection rate to account for fear in periodic environments. The model's equilibrium solutions are identified, and stability analysis is conducted. The impact of vital parameters on disease progression is determined via sensitivity analysis and numerical simulations. The study highlights the significance of fear and seasonality in disease transmission and emphasizes the implications for public health resulting from the findings. Pitzer et al. [22] developed a non-autonomous mathematical model to elucidate patterns in TyF cases in Blantyre, Malawi. The findings indicate that before 2010, the transmission was mainly influenced by chronic carriers and sub-critical transmission from primary infections. However, the appearance of multidrug-resistant strains and the H58 haplotype allowed the disease to infect more than one person, resulting in exponential epidemic growth.

This study builds upon prior research conducted in papers such as [18,22,23]. These studies have laid the foundation for our work by establishing mathematical models and analyzing various aspects of typhoid fever transmission. In our research, we construct a non-autonomous compartmental model that considers the impact of periodic environmental changes, specifically incorporating seasonal variations in transmission rates based on rainfall. This extension goes beyond the scope of [18], which did not include environmental periodicity. Furthermore, in contrast to [22], we focus on analyzing \mathcal{R}_0 , the basic reproduction number, for our periodic model to investigate its dynamics. We establish the global asymptotic stability (GAS) of disease-free periodic solution (DFPS) and the existence of periodic solutions, varying with \mathcal{R}_0 . Additionally, we perform numerical simulations to validate our findings. In particular, our investigation examines how the transmission dynamics of TyF are affected by various factors, such as the seasonal transmission rate, rates of bacteria extraction and decay, proportion of chronic carriers, and other important parameters. In our analysis of the time-periodic model, we utilize approaches established and applied in previous studies on periodic epidemic models. Specifically, we draw upon the techniques used in [23–27].

The article is structured into different sections, starting with Section 2, which details the proposed model. Section 3 focuses on determining reproduction numbers, while Section 4 presents the global dynamics in relation to \mathcal{R}_0 . Finally, Section 5 contains numerical simulation results.

2. Typhoid Compartmental Model Formulation

Our model classifies the human population into nine compartments and two sub-populations based on their level of infection: primary infected and partially infected. The model that we propose, represented by Equation (1), builds upon prior models such as those presented in [18,22], as well as other models concerning the transmission dynamics of TyF. Specifically, our model incorporates a seasonal transmission parameter. To put it simply, the model postulates that people are naturally vulnerable to being infected and developing illness due to *Salmonella Typhi* ($S_1(t)$). Those susceptible to the infection can acquire it through either human-to-human transmission (direct or short-cycle) or environment-to-human transmission (indirect or long-cycle) and then move to the exposed class ($E_1(t)$), where they remain exposed for a period of $1/\nu$. People who contract the primary infection ($I_1(t)$) stay contagious for a period of $1/\delta$. After that period, we presume that a portion (α) of them will die due to the illness, while another portion (θ) develop gallbladder infections and become chronic carriers ($C(t)$) [6,7]. The remaining individuals, comprising of $(1 - \theta - \alpha)$, will undergo recovery and attain temporary immunity ($R(t)$). We hypothesize that $\alpha + \theta \leq 1$ and the value of θ varies depending on the infected person's age, which is supported by epidemiological evidence [28]. At a certain rate ω , a person's immunity against future infections decreases, making them partially susceptible ($S_2(t)$). In the event of reinfection, before the partial immunity wanes at a rate of η , these partially susceptible individuals move into the exposed class ($E_2(t)$), where they remain exposed for a duration of $1/\nu$. After that period, any subsequent reinfection ($I_2(t)$) is assumed to be sub-clinical. Infected individuals who experience sub-clinical infections can either recover or become chronic carriers. $B(t)$ is used to represent the density of bacteria in the environment. It is assumed that all individuals who are infected with the pathogen release bacteria into the environment's reservoir ($B(t)$) at a rate of γ . The infectious period of these bacteria lasts for a duration of $1/\xi$. Additionally, the infectiousness of individuals who are chronic carriers is reduced by a factor of $\tau \leq 1$. Therefore, susceptible humans become infectious at a rate of $(\beta\lambda(t) + \beta_b(t))S_i$ for $i = 1$ or 2 , where $\lambda(t) = I_1(t) + I_2(t) + \tau C(t)$. The parameters β and $\beta_b(t)$ represent the rate of infection from infected to susceptible humans and the rate of infection from the environment to susceptible humans, respectively. TyF transmission can be seasonal in some regions, particularly in areas with monsoon seasons, due to factors such as flooding and poor sanitation. However, the seasonality of TyF transmission can vary depending on the geographic location and local environmental

factors. Based on this information, we made an assumption in our model that $\beta_b(t)$ is a continuous, positive T-periodic function to represent the seasonal transmission of the disease. The diagram in Figure 1 provides an illustration of the model.

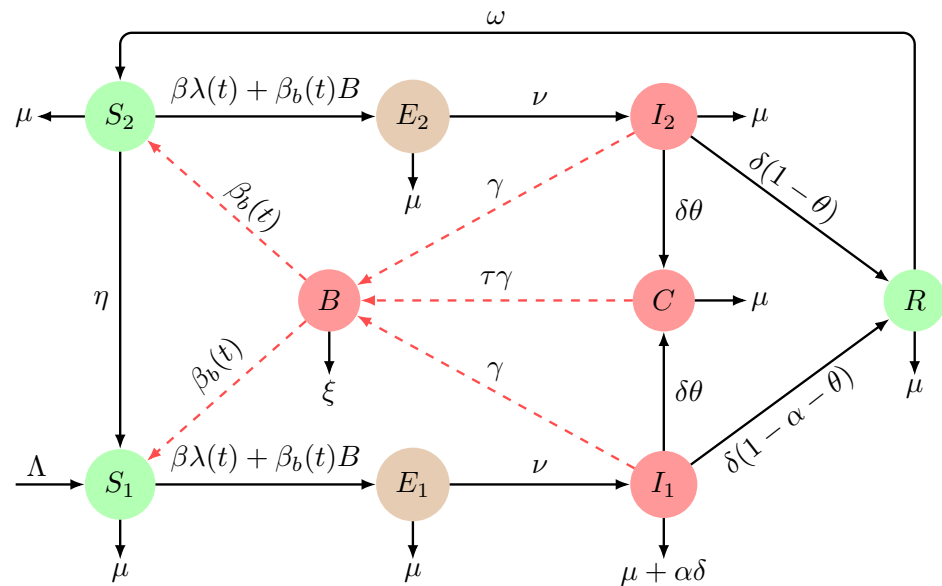


Figure 1. Diagram illustrating the flow of the model (1). The red and brown nodes represent infectious individuals, and the green nodes represent non-infectious individuals. The black solid arrows indicate the progression of infection, while the red dashed arrows represent the direction of transmission between humans and bacteria.

Using the notations introduced above and Figure 1, we can express our model equations as follows:

$$\begin{aligned}
 S_1'(t) &= \Lambda - \beta\lambda(t)S_1(t) - \beta_b(t)B(t)S_1(t) + \eta S_2(t) - \mu S_1(t), \\
 E_1'(t) &= \beta\lambda(t)S_1(t) + \beta_b(t)B(t)S_1(t) - \nu E_1(t) - \mu E_1(t), \\
 I_1'(t) &= \nu E_1(t) - (\delta + \mu)I_1(t), \\
 R'(t) &= \delta(1 - \alpha - \theta)I_1(t) + \delta(1 - \theta)I_2(t) - \omega R(t) - \mu R(t), \\
 C'(t) &= \delta\theta I_1(t) + \delta\theta I_2(t) - \mu C(t), \\
 S_2'(t) &= \omega R(t) - \beta\lambda(t)S_2(t) - \beta_b(t)B(t)S_2(t) - \eta S_2(t) - \mu S_2(t), \\
 E_2'(t) &= \beta\lambda(t)S_2(t) + \beta_b(t)B(t)S_2(t) - \nu E_2(t) - \mu E_2(t), \\
 I_2'(t) &= \nu E_2(t) - (\delta + \mu)I_2(t), \\
 B'(t) &= \gamma\lambda(t) - \xi B(t).
 \end{aligned}
 \tag{1}$$

For clarity, we have provided a summary of the model parameters in Table 1.

Table 1. Model (1) parameters and description.

Parameters	Description
Λ, μ	Human birth and mortality rates
β	Infected-to-susceptible infection rate
$\beta_b(t)$	Environment-to-susceptible infection rate
γ	Bacteria excretion
ν	Rate of progression to carriers
θ	Proportion infected who transition into chronic carriers
$1/\delta$	Duration of infectiousness
α	Disease-induced mortality
$1/\omega$	Temporary full-immunity duration to infection
τ	Relative infectiousness of chronic carriers
η	Immunity waning rate to clinical disease
ξ	Bacterial decay rate

2.1. Basic Properties

Our initial focus is to investigate whether the solutions for Equation (1) exist and are unique. To facilitate our analysis, we will introduce some notation.

$$(S_1(0), E_1(0), I_1(0), R(0), C(0), S_2(0), E_2(0), I_2(0), B(0)) = (S_1^0, E_1^0, I_1^0, R^0, C^0, S_2^0, E_2^0, I_2^0, B^0) \in \mathbb{R}_+^9,$$

where \mathbb{R}_+ is the set of non-negative real numbers. It follows from ([29], Theorem 5.2.1) that Model (1) has single non-negative local solution

$$(S_1(t), E_1(t), I_1(t), R(t), C(t), S_2(t), E_2(t), I_2(t), B(t)),$$

for any initial value $(S_1^0, E_1^0, I_1^0, R^0, C^0, S_2^0, E_2^0, I_2^0, B^0) \in \mathbb{R}_+^9$. For the human subsystem of (1) with a positive initial condition, let

$$N(t) = S_1(t) + E_1(t) + I_1(t) + R(t) + C(t) + S_2(t) + E_2(t) + I_2(t).$$

Then, $N(t)$ satisfies

$$N'(t) = \Lambda - \mu N(t) - \delta I_1(t) - \delta I_2(t) \leq \Lambda - \mu N(t). \tag{2}$$

Therefore,

$$\overline{\lim}_{t \rightarrow \infty} N(t) \leq \frac{\Lambda}{\mu}, \tag{3}$$

where the notation $\overline{\lim}_{t \rightarrow \infty}$ (or \limsup), represents the limit superior as t approaches infinity. Assuming the absence of the disease in the population, Equation (2) has a unique equilibrium $N^* = \Lambda/\mu$ that is GAS. Additionally, $N(t)$ is bounded.

By applying the aforementioned inequality, we can derive from the last equation in (1) that $I_1 + I_2 + \tau C \leq I_1 + I_2 + C \leq N \leq \frac{\Lambda}{\mu}$, and

$$B'(t) \leq \frac{\gamma \Lambda}{\mu} - \xi B(t). \tag{4}$$

Solving the above Equation (4) gives $B(t) \leq \frac{\gamma \Lambda}{\xi \mu} + B^0 e^{-\xi t}$, which implies that B is non-negative. Therefore, by applying the limit to the previous inequality, we obtain

$$\overline{\lim}_{t \rightarrow \infty} B(t) \leq \frac{\gamma \Lambda}{\xi \mu}, \tag{5}$$

and hence $B(t)$ remains bounded as well. Consequently, the preceding discussion indicates that system (1) solutions are bounded and non-negative within the given region

$$\Omega := \left\{ (S_1, E_1, I_1, R, C, S_2, E_2, I_2, B) \in \mathbb{R}_+^9 : N \leq \frac{\Lambda}{\mu}, B \leq \frac{\gamma\Lambda}{\xi\mu} \right\}.$$

As a consequence, we state the following proposition:

Proposition 1. *System (1) is positively invariant with respect to the region Ω . Specifically, if the initial values $(S_1^0, E_1^0, I_1^0, R^0, C^0, S_2^0, E_2^0, I_2^0, B^0) \in \mathbb{R}_+^9$ at time $t = 0$, then the solution $(S_1(t), E_1(t), I_1(t), R(t), C(t), S_2(t), E_2(t), I_2(t), B(t))$ is positive for all $t > 0$.*

Proof. In order to establish that the solutions of (1) are non-negative, it is enough to demonstrate that the solution components $(S_1(t), E_1(t), I_1(t), R(t), C(t), S_2(t), E_2(t), I_2(t), B(t)) \geq 0$ for all $t > 0$, given that $(S_1^0, E_1^0, I_1^0, R^0, C^0, S_2^0, E_2^0, I_2^0, B^0) \in \mathbb{R}_+^9$. Let $q(t)$ be defined as the minimum value among $\{S_1(t), E_1(t), I_1(t), R(t), C(t), S_2(t), E_2(t), I_2(t), B(t)\}$ for all $t > 0$. Assuming that $q(0) > 0$, we can infer the existence of $t_1 > 0$ such that $q(t_1) = 0$, while ensuring that $q(t) \geq 0$ for all $t \in [0, t_1]$. Given the assumption that $q(t_1) = S_i(t_1)$, where $i = 1$ or 2 , we can derive the following inequalities from System (1) for all $t \in [0, t_1]$:

$$S_i'(t) \geq -(\beta\lambda(t) + \beta_b(t)B(t) + \mu)S_i(t).$$

From these inequalities, we can observe that at $t = t_1$, the condition $0 = S_i(t_1) \geq S_i^0 e^{-\int_0^{t_1} (\beta\lambda(s) + \beta_b(s)B(s) + \mu) ds} > 0$ holds. The impossibility of $S_i(t)$ having negative values for any $t > 0$ leads to this contradiction. Assuming the rest of the human equations in (1), we can make the assumption that there exists a minimum time value $t > 0$ where one of the compartments, specifically $E_1(t), I_1(t), R(t), C(t), E_2(t)$, or $I_2(t)$, becomes zero. Let us consider, without any loss of generality, that this specific compartment is $E_i(t)$, where $i = 1$ or 2 . In the case where $q(t_1) = E_i(t_1)$, the following inequalities are derived:

$$E_i'(t) \geq -(v + \mu)E_i(t), \quad \forall t \in [0, t_1].$$

Based on this inequalities, if $0 = E_i(t_1) \geq E_i^0 e^{-(v+\mu)t_1} > 0$, we arrive at a contradiction. Similarly, if $q(t_1)$ is equal to any of the variables $I_1(t_1), R(t_1), C(t_1)$, or $I_2(t_1)$, we can reach a similar contradiction. Hence, $S_1(t) \geq 0, E_1(t) \geq 0, I_1(t) \geq 0, R(t) \geq 0, C(t) \geq 0, S_1(t) \geq 0, E_2(t) \geq 0$, and $I_2(t) \geq 0$ for all $t > 0$. Furthermore, equality is present if the initial values are set to zero. The inequalities (3) and (5) indicate that for all $t > 0$ both $N(t)$ and $B(t)$ are bounded. This observation concludes the proof. \square

2.2. Disease-Free Solution

The disease-free periodic solution (DFPS) of (1) is provided when there is no presence of disease by

$$\mathbf{P}^* = (S_1^*, E_1^*, I_1^*, R^*, C^*, S_2^*, E_2^*, I_2^*, B^*) = \left(\frac{\Lambda}{\mu}, 0, 0, 0, 0, 0, 0, 0, 0\right), \tag{6}$$

and it is always feasible. In Section 4, we will study the global dynamic of \mathbf{P}^* based on \mathcal{R}_0 of periodic epidemic models.

3. Reproduction Numbers

Within this section, our primary objective is to calculate \mathcal{R}_0 , the basic reproduction number (BRNP) for the periodic system described by Equation (1). Additionally, we will derive an expression of \mathcal{R}_0^A , representing the basic reproduction rate (BRNA) for the autonomous model derived from the system defined by Equation (1). Furthermore, we will compute, $[\mathcal{R}_0]$, the time average reproduction rate (BRNT) corresponding to Equation (1).

3.1. Basic Reproduction Number (BRNP) of the Model (1)

Using the approach proposed by Wang and Zhao [25], we will determine the BRNP \mathcal{R}_0 for the model (1).

The vector $\mathbf{Y} = (E_1, I_1, E_2, I_2, C, B, S_1, S_2, R)^T$ represents the state of a system, where $\mathbf{F}(t, \mathbf{Y}(t))$, $\mathbf{V}^+(t, \mathbf{Y}(t))$, and $\mathbf{V}^-(t, \mathbf{Y}(t))$ are the rates of newly infected individuals, individuals from other sources, and individuals transferred out of compartments, respectively. To ensure the fulfillment of the conditions (A1)–(A7) in ([25], Section 1), we have restructured system (1), which can be expressed as the following non-autonomous equation:

$$\mathbf{Y}'(t) = \mathbf{F}(t, \mathbf{Y}(t)) - \mathbf{V}(t, \mathbf{Y}(t)), \tag{7}$$

where $\mathbf{V}(t, \mathbf{Y}(t)) = \mathbf{V}^-(t, \mathbf{Y}(t)) - \mathbf{V}^+(t, \mathbf{Y}(t))$. The DFPS of (7) is defined by $\mathbf{Y}^* = (0, 0, 0, 0, 0, 0, S_1^*, 0, 0)$. To compute the matrices $\mathcal{F}(t)$ and $\mathcal{V}(t)$, we define $\mathcal{F}(t)$ as the matrix $(\frac{\partial \mathbf{F}_i(t, \mathbf{Y}^*)}{\partial \mathbf{Y}_j})_{1 \leq i, j \leq 6}$ and the matrix $\mathcal{V}(t)$ is defined as $(\frac{\partial \mathbf{V}_i(t, \mathbf{Y}^*)}{\partial \mathbf{Y}_j})_{1 \leq i, j \leq 6}$. The entries of $\mathcal{F}(t)$ and $\mathcal{V}(t)$ expressed as

$$\mathcal{F}(t) = \begin{bmatrix} 0 & \beta S_1^* & 0 & \beta S_1^* & \beta \tau S_1^* & \beta_b(t) S_1^* \\ 0 & 0 & 0 & 0 & 0 & 0 \\ 0 & 0 & 0 & 0 & 0 & 0 \\ 0 & 0 & 0 & 0 & 0 & 0 \\ 0 & 0 & 0 & 0 & 0 & 0 \\ 0 & 0 & 0 & 0 & 0 & 0 \end{bmatrix},$$

and

$$\mathcal{V}(t) = \begin{bmatrix} \nu + \mu & 0 & 0 & 0 & 0 & 0 \\ -\nu & \alpha \delta + \mu & 0 & 0 & 0 & 0 \\ 0 & 0 & \nu + \mu & 0 & 0 & 0 \\ 0 & 0 & -\nu & \delta + \mu & 0 & 0 \\ 0 & -\delta \theta & 0 & -\delta \theta & \mu & 0 \\ 0 & -\gamma & 0 & -\gamma & -\gamma \tau & \xi \end{bmatrix}.$$

Conditions (A1) through (A6) given in [25] are simple to confirm, and the disease-free subspace \mathbf{Y}^* is linearly asymptotically stable at $\mathbf{Y}_s = (0, 0, 0, 0, 0, 0, S_1, S_2, R) \in \mathbb{R}_+^9$.

Assuming $\mathbf{Z}(s_1, s_2)$ is a solution to the IVP (initial value problem) below with $s_1 \geq s_2$:

$$\frac{d\mathbf{Z}(s_1, s_2)}{dt} = -\mathcal{V}(s_1)\mathbf{Z}(s_1, s_2), \quad \mathbf{Z}(s_2, s_2) = I_6, \quad \forall s_1 \geq s_2, \tag{8}$$

where I_6 denotes the identity matrix (6×6). Hence, the requirement (A7) given in [25] is satisfied since the matrix $\Phi_{-\mathcal{V}}(t)$ of (8) for $t \geq 0$ is equivalent to $\mathbf{Z}(s, 0)$. Let us denote the ordered Banach space of T -periodic functions from \mathbb{R} to \mathbb{R}^6 by \mathcal{C}_T with $\|\cdot\|_\infty$ (usual maximum norm) and define $\mathcal{C}_T^+ := \{\phi \in \mathcal{C}_T : \phi(t) \geq 0, \forall t \in \mathbb{R}\}$ (positive cone).

The linear operator \mathbf{K} for subsequent infections maps \mathcal{C}_T to \mathcal{C}_T . Its definition is given by

$$(\mathbf{K}\phi)(s) = \int_0^\infty \mathbf{Z}(s, s-r)\mathcal{F}(s-r)\phi(s-r)dr, \quad \forall \phi \in \mathcal{C}_T, s \in \mathbb{R}.$$

The BRNP \mathcal{R}_0 of the model (1) can be determined as the spectral radius of \mathbf{K} ; therefore,

$$\mathcal{R}_0 := \rho(\mathbf{K}). \tag{9}$$

Let $\Phi_{\mathcal{F}-\mathcal{V}}(t)$ is a fundamental matrix of the linear T -periodic system $\mathbf{x}' = [\mathcal{F}(t) - \mathcal{V}(t)]\mathbf{x}$. In addition, and without loss of generality, we assume that $\Phi_{\mathcal{F}-\mathcal{V}}(0) = I$, namely, the identity matrix. Now, at this step, we recall that $\Phi_{\mathcal{F}-\mathcal{V}}(T)$ is the monodromy matrix of the linear T -periodic system above mentioned. We will need the following Theorem 2.2 from [25] for the local stability of \mathbf{P}^* defined in (6).

Theorem 1. *The relation between the BRNP and the monodromy matrix is described as follows.*

1. $\mathcal{R}_0 = 1$ is the same as $\rho(\Phi_{\mathcal{F}-\mathcal{V}}(T)) = 1$;
2. $\mathcal{R}_0 > 1$ is the same as $\rho(\Phi_{\mathcal{F}-\mathcal{V}}(T)) > 1$;
3. $\mathcal{R}_0 < 1$ is the same as $\rho(\Phi_{\mathcal{F}-\mathcal{V}}(T)) < 1$.

The inequalities stated in the Theorem 1 are equivalent to the stability of the origin of the periodic system $x' = [\mathcal{F}(t) - \mathcal{V}(t)]x$ described by the classical Floquet’s theory.

3.2. Basic Reproduction Number (BRNA) of the Constant Model

If we have $\beta_b(t) = \bar{\beta}_b$ for $\forall t \geq 0$, which leads to $\mathcal{F}(t) \equiv \mathcal{F}$, we can use the findings of [30] study to calculate \mathcal{R}_0^A for the autonomous version of model (1) as follows:

$$\mathcal{R}_0^A = \frac{\nu(\beta\bar{\zeta} + \bar{\beta}_b\gamma)(\delta\theta\tau + \mu)S_1^*}{\mu\bar{\zeta}(\mu + \nu)(\alpha\delta + \mu)} = \frac{\nu\beta(\delta\theta\tau + \mu)S_1^*}{\mu(\mu + \nu)(\alpha\delta + \mu)} + \frac{\nu\bar{\beta}_b\gamma(\delta\theta\tau + \mu)S_1^*}{\mu\bar{\zeta}(\mu + \nu)(\alpha\delta + \mu)}. \tag{10}$$

The BRNA \mathcal{R}_0^A can be expressed as the sum of two components: the reproductive number for short-period infections, denoted as \mathcal{R}_{0h} , and the reproductive number for long-period infections, denoted as \mathcal{R}_{0b} , where

$$\mathcal{R}_{0h} = \frac{\nu\beta(\delta\theta\tau + \mu)S_1^*}{\mu(\mu + \nu)(\alpha\delta + \mu)} \quad \text{and} \quad \mathcal{R}_{0b} = \frac{\nu\bar{\beta}_b\gamma(\delta\theta\tau + \mu)S_1^*}{\mu\bar{\zeta}(\mu + \nu)(\alpha\delta + \mu)}.$$

Remark 1. *We define the integral average of a continuous function $f(t)$, where $f(t)$ is T -periodic. Using the notation presented in [23,31], we denote the integral average as $[f] := \frac{1}{T} \int_0^T f(t) dt$.*

Therefore, $[\mathcal{R}_0]$ for the corresponding time-varying model is expressed as follows:

$$[\mathcal{R}_0] = \frac{\nu(\beta\bar{\zeta} + [\beta_b]\gamma)(\delta\theta\tau + \mu)S_1^*}{\mu\bar{\zeta}(\mu + \nu)(\alpha\delta + \mu)}, \tag{11}$$

where

$$\mathcal{R}_{0h} = \frac{\nu\beta(\delta\theta\tau + \mu)S_1^*}{\mu(\mu + \nu)(\alpha\delta + \mu)} \quad \text{and} \quad [\mathcal{R}_{0b}] = \frac{\nu[\beta_b]\gamma(\delta\theta\tau + \mu)S_1^*}{\mu\bar{\zeta}(\mu + \nu)(\alpha\delta + \mu)}.$$

4. Threshold Dynamics

This section aims to demonstrate that the DFPS \mathbf{P}^* , defined in (6), is GAS and that the disease goes extinct when the BRNP \mathcal{R}_0 is less than 1. On the other hand, if \mathcal{R}_0 is greater than 1, we will prove the persistence of disease and the existence of a positive periodic solution for (1). Throughout this section, the BRNP \mathcal{R}_0 is defined as shown in Equation (9). To establish the GAS of the DFPS \mathbf{P}^* and the persistence of TyF, we will require the following lemma.

Lemma 1 ([32], Lemma 2.1). *Consider $\zeta = \frac{1}{T} \ln \rho(\Phi_{D(\cdot)}(T))$. With this consideration, there exists a function $u(t) > 0$ with a period of T where $e^{\zeta t}u(t) > 0$ becomes a solution to the problem $z' = D(t)z$.*

4.1. Local Stability of the DFPS \mathbf{P}^*

Building upon the previous results in Section 3, we state the subsequent Theorem regarding the local asymptotic stability (LAS) of \mathbf{P}^* defined in (6) of the model (1).

Theorem 2. *In the case where $\mathcal{R}_0 < 1$, the DFPS \mathbf{P}^* defined in (6) demonstrates local asymptotic stability. On the other hand, when $\mathcal{R}_0 > 1$, \mathbf{P}^* is unstable.*

Proof. The matrix $\mathcal{J}(t)$, which represents the Jacobian of the system described by Equation (1) at \mathbf{P}^* , can be defined as $\mathcal{J}(t) = \begin{bmatrix} \mathcal{F}(t) - \mathcal{V}(t) & 0 \\ -\mathcal{A}(t) & M \end{bmatrix}$, where $\mathcal{A}(t)$ and M are given by

$$\mathcal{A}(t) = \begin{bmatrix} 0 & \beta S_1^* & 0 & \beta S_1^* & \beta \tau S_1^* & \beta_b(t) S_1^* \\ 0 & 0 & 0 & 0 & 0 & 0 \\ 0 & -\delta(1 - \alpha - \theta) & 0 & -\delta(1 - \theta) & 0 & 0 \end{bmatrix},$$

and

$$M = \begin{bmatrix} -\mu & \eta & 0 \\ 0 & -(\eta + \mu) & \omega \\ 0 & 0 & -(\omega + \mu) \end{bmatrix}.$$

The matrix M is a fixed matrix with eigenvalues $-\mu$, $-\eta - \mu$, and $-\omega - \mu$. As all eigenvalues of M are negative, we can observe that $\rho(\Phi_M) < 1$. The conditions $\rho(\Phi_{\mathcal{F}-\mathcal{V}}(T)) < 1$ and $\rho(\Phi_M(T)) < 1$ determine the LAS of \mathbf{P}^* according to the findings in [33]. Hence, the stability of the DFPS \mathbf{P}^* relies solely on the value of $\rho(\Phi_{\mathcal{F}-\mathcal{V}}(T))$. Consequently, \mathbf{P}^* is unstable if $\rho(\Phi_{\mathcal{F}-\mathcal{V}}(T)) > 1$, and it becomes LAS if $\rho(\Phi_{\mathcal{F}-\mathcal{V}}(T)) < 1$. The proof is completed by the finding of Theorem 1. \square

4.2. Global Stability of the DFPS \mathbf{P}^*

Theorem 3. *In the case, $\mathcal{R}_0 < 1$, the DFPS \mathbf{P}^* exhibits global asymptotic stability.*

Proof. Based on the local stability analysis in Theorem 2, if $\mathcal{R}_0 < 1$, the DFPS \mathbf{P}^* is LAS. It is still necessary to demonstrate that \mathbf{P}^* is globally attractive. The requirements (A1) through (A7) described in [24] are met, according to the discussion in Section 3. Furthermore, $\mathbf{Y}^* = (0, 0, 0, 0, 0, 0, S_1^*, 0, 0)$ represents the single periodic solution of (7) within the set of disease-free states \mathbf{Y}_s . Taking the first equation of (1), we obtain the following expression:

$$S_1'(t) = \Lambda - \beta\lambda(t)S_1(t) - \beta_b(t)B(t)S_1(t) + \eta S_2(t) - \mu S_1(t).$$

Because $I_1(t) \geq 0$, $I_2(t) \geq 0$ and $B(t) \geq 0$, One can prove that $S_1'(t) \leq \Lambda - \mu S_1(t)$, meaning that

$$\overline{\lim}_{t \rightarrow \infty} S_1(t) \leq \frac{\Lambda}{\mu} = S_1^*.$$

Thus, there is a $t(\epsilon) > 0$ where $S_1(t) \leq S_1^* + \epsilon$ and $S_2(t) \leq S_2^* + \epsilon$ for all $t > t(\epsilon)$, for an arbitrary $\epsilon > 0$. Referring back to (1), for $t > t(\epsilon)$, we have

$$\begin{aligned} E_1'(t) &\leq (\beta\lambda(t) + \beta_b(t)B(t))(S_1^* + \epsilon) - \nu E_1(t) - \mu E_1(t), \\ I_1'(t) &\leq \nu E_1(t) - (\delta + \mu)I_1(t), \\ E_2'(t) &\leq (\beta\lambda(t) + \beta_b(t)B(t))(S_2^* + \epsilon) - \nu E_2(t) - \mu E_2(t), \\ I_2'(t) &\leq \nu E_2(t) - (\delta + \mu)I_2(t), \\ C'(t) &\leq \delta\theta I_1(t) + \delta\theta I_2(t) - \mu C(t), \\ B'(t) &\leq \gamma\lambda(t) - \zeta B(t). \end{aligned}$$

We define $\mu(\epsilon) := \min\{S_1^*/(S_1^* + \epsilon), S_2^*/(S_2^* + \epsilon)\}$, which leads us to the system:

$$H'(t) \leq \left(\frac{\mathcal{F}(t)}{\mu(\epsilon)} - \mathcal{V}(t)\right)H(t), \quad \forall t \geq t(\epsilon), \tag{12}$$

with $H(t) = (E_1(t), I_1(t), E_2(t), I_2(t), C(t), B(t))$. As t approaches infinity, $H(t)$ tends to zero, leading to the extinction of the disease. The application of ([24], Theorem 2) allows us to deduce that \mathbf{Y}^* achieves GAS by virtue of its GAS behavior within the disease-free subspace \mathbf{Y}_s . \square

4.3. Persistence

The objective of this subsection is to illustrate the persistence of infectious compartments when $\mathcal{R}_0 > 1$ through the application of the general technique introduced by [24]. Let $S = S_1 + S_2, E = E_1 + E_2$ and $I = I_1 + I_2$. Then, (1) can be expressed as follows:

$$\begin{aligned}
 S'(t) &= \Lambda - \beta\lambda(t)S(t) - \beta_b(t)B(t)S(t) - \mu S + \omega R(t), \\
 E'(t) &= \beta\lambda(t)S(t) + \beta_b(t)B(t)S(t) - \nu E(t) - \mu E(t), \\
 I'(t) &= \nu E(t) - (\delta + \mu)I(t), \\
 R'(t) &= \delta(1 - \theta)I(t) - \delta\alpha I_1(t) - \omega R(t) - \mu R(t), \\
 C'(t) &= \delta\theta I - \mu C(t), \\
 B'(t) &= \gamma\lambda(t) - \zeta B(t).
 \end{aligned}
 \tag{13}$$

In the following, we demonstrate the persistence of the infected compartments within (13).

Theorem 4. *Assuming $\mathcal{R}_0 > 1$, the system (13) exhibits persistence concerning the variables E, I, C , and B .*

Proof. The persistence of $E + I$ indicates the persistence of both E and I and, consequently, the persistence of C and B as well. Suppose there exists a positive value ε where $\liminf_{t \rightarrow +\infty} (E + I) \geq \varepsilon$. In that case, for large t , it follows that $E \geq \frac{\varepsilon}{2} - I$. Based on system (13), we obtain $I'(t) \geq \nu \frac{\varepsilon}{2} - (\delta + \mu)I(t)$. Therefore, we can conclude that

$$I(t) \geq \frac{\nu\varepsilon}{2(\delta + \mu)} =: \kappa_i(\varepsilon).
 \tag{14}$$

By substituting into the fifth equation of (13), we can derive that $C'(t) \geq \delta\theta\kappa_i(\varepsilon) - \mu C(t)$. We obtain

$$C(t) \geq \frac{\delta\theta\kappa_i(\varepsilon)}{\mu} =: \kappa_c(\varepsilon).
 \tag{15}$$

By incorporating the inequalities (14) and (15) into the final equation of system (13), we obtain that $B'(t) \geq \gamma(\kappa_i(\varepsilon) + \tau\kappa_c(\varepsilon)) - \zeta B(t)$, and hence,

$$B(t) \geq \frac{\kappa_i(\varepsilon) + \tau\kappa_c(\varepsilon)}{\zeta} =: \kappa_b(\varepsilon).
 \tag{16}$$

Suppose that $E \leq \varepsilon, I \leq \varepsilon, C \leq \varepsilon, R \leq \varepsilon$, and $B \leq \varepsilon$ for all $t \geq t_0$. Then, there exists $t_1 \geq t_0$ such that $|N(t) - S^*| \leq \varepsilon$ for all $t \geq t_1$ and $S^* = S_1^* + S_2^* = S_1^*$. Hence, for all $t \geq t_1$, we have $S(t) = N(t) - E(t) - I(t) - C(t) - R(t) \geq S^* - 4\varepsilon$. Set $\lambda(\varepsilon) := \max\{S^*/(S^* - 4\varepsilon)\}$. Then, using the models' equations, for fairly large $t \geq t_1$, one can derive:

$$\begin{aligned}
 E'(t) &\geq (\beta\lambda(t) + \beta_b(t)B(t)) \frac{S^*}{\lambda(\varepsilon)} - \nu E(t) - \mu E(t), \\
 I'(t) &\geq \nu E(t) - (\delta + \mu)I(t), \\
 C'(t) &\geq \delta\theta I - \mu C(t), \\
 B'(t) &\geq \gamma\lambda(t) - \zeta B(t).
 \end{aligned}$$

Therefore, the assumptions of ([24], Theorem 4) are met and (13) is persistent with respect to E, I, C , and B . \square

4.4. Existence of Endemic Periodic Solutions

We will proceed by introducing the following symbols/notations:

$$\begin{aligned}
 X &:= \left\{ (S_1, E_1, I_1, R, C, S_2, E_2, I_2, B) \in \mathbb{R}_+^9 \right\}, \\
 X_0 &:= \left\{ (S_1, E_1, I_1, R, C, S_2, E_2, I_2, B) \in X : E_1 > 0, I_1 > 0, C > 0, E_2 > 0, I_2 > 0, B > 0 \right\}, \\
 \text{and} \\
 \partial X_0 &:= X \setminus X_0 = \left\{ (S_1, E_1, I_1, R, C, S_2, E_2, I_2, B) \in X : E_1 I_1 C E_2 I_2 B = 0 \right\}.
 \end{aligned}$$

The function $\mathcal{P} : \mathbb{R}_+^9 \rightarrow \mathbb{R}_+^9$ is defined as the Poincaré map associated with (1). Specifically, we define $\mathcal{P}(x^0)$ as the function $u(T, x^0)$ for $x^0 \in \mathbb{R}_+^9$, and $u(t, x^0)$ represents the unique solution of the (1) with the initial condition x^0 . It follows that, for all $m \geq 0$, we have $\mathcal{P}^m(x^0) = u(mT, x^0)$.

Lemma 2. For any $(S_1^0, E_1^0, I_1^0, R^0, C^0, S_2^0, E_2^0, I_2^0, B^0) \in X_0$ with $\|(S_1^0, E_1^0, I_1^0, R^0, C^0, S_2^0, E_2^0, I_2^0, B^0) - \mathbf{P}^*\| \leq \sigma$, where $\sigma > 0$, if $\mathcal{R}_0 > 1$, then the following inequality holds:

$$\overline{\lim}_{m \rightarrow \infty} d(\mathcal{P}^m(S_1^0, E_1^0, I_1^0, R^0, C^0, S_2^0, E_2^0, I_2^0, B^0), \mathbf{P}^*) \geq \sigma.$$

Proof. Applying Theorem 1, it can be concluded that $\rho(\Phi_{\mathcal{F}-\mathcal{V}}(T)) > 1$ when \mathcal{R}_0 is greater than 1. Therefore, there is a small enough $\varrho > 0$ such that $\rho(\Phi_{\mathcal{F}-\mathcal{V}-M_\varrho}(T)) > 1$, where $M_\varrho(t)$ is given by

$$\begin{bmatrix}
 0 & \beta\varrho & 0 & \beta\varrho & \beta\tau\varrho & \beta_b(t)\varrho \\
 0 & 0 & 0 & 0 & 0 & 0 \\
 0 & 0 & 0 & 0 & 0 & 0 \\
 0 & \beta\varrho & 0 & \beta\varrho & \beta\tau\varrho & \beta_b(t)\varrho \\
 0 & 0 & 0 & 0 & 0 & 0 \\
 0 & 0 & 0 & 0 & 0 & 0
 \end{bmatrix}.$$

Let $\varrho > 0$ be an arbitrary constant. There exists a positive constant $\sigma = \sigma(\varrho)$ such that for any $x^0 = (S_1^0, E_1^0, I_1^0, R^0, C^0, S_2^0, E_2^0, I_2^0, B^0) \in X_0$ satisfying $\|x^0 - \mathbf{P}^*\| \leq \sigma$, the continuous dependence of solutions on their initial values ensures that the following inequality holds:

$$\|u(t, (S_1^0, E_1^0, I_1^0, R^0, C^0, S_2^0, E_2^0, I_2^0, B^0)) - u(t, \mathbf{P}^*)\| \leq \varrho, \quad 0 \leq t \leq T.$$

Our next claim is that

$$\overline{\lim}_{m \rightarrow \infty} d(\mathcal{P}^m(S_1^0, E_1^0, I_1^0, R^0, C^0, S_2^0, E_2^0, I_2^0, B^0), \mathbf{P}^*) \geq \sigma. \tag{17}$$

Assuming that (17) is not satisfied, we have

$$\overline{\lim}_{m \rightarrow \infty} d(\mathcal{P}^m(S_1^0, E_1^0, I_1^0, R^0, C^0, S_2^0, E_2^0, I_2^0, B^0), \mathbf{P}^*) < \sigma, \tag{18}$$

holds for some $(S_1^0, E_1^0, I_1^0, R^0, C^0, S_2^0, E_2^0, I_2^0, B^0) \in X_0$. We can make the simplifying assumption that

$$d(\mathcal{P}^m(S_1^0, E_1^0, I_1^0, R^0, C^0, S_2^0, E_2^0, I_2^0, B^0), \mathbf{P}^*) < \sigma, \quad \forall m \geq 0.$$

The preceding information indicates

$$\|u(t, \mathcal{P}^m(S_1^0, E_1^0, I_1^0, R^0, C^0, S_2^0, E_2^0, I_2^0, B^0)) - u(t, \mathbf{P}^*)\| < \varrho, \quad \forall 0 \leq t \leq T, \quad m \geq 0.$$

Let $t \geq 0$ be expressed as $t = t_1 + mT$, where $0 \leq t_1 < T$ and $m = [\frac{t}{T}]$, denoting the greatest integer not exceeding $\frac{t}{T}$. By employing this representation, we obtain

$$\|u(t, (S_1^0, E_1^0, I_1^0, R^0, C^0, S_2^0, E_2^0, I_2^0, B^0)) - u(t, \mathbf{P}^*)\|$$

$$= \|u(t_1, \mathcal{P}^m(S_1^0, E_1^0, I_1^0, R^0, C^0, S_2^0, E_2^0, I_2^0, B^0)) - u(t_1, \mathbf{P}^*)\| < \varrho,$$

for all $t \geq 0$, suggesting that $S_1(t) \geq S_1^* - \varrho$ and $S_2(t) \geq S_2^* - \varrho$. Then, for

$$\|(S_1^0, E_1^0, I_1^0, R^0, C^0, S_2^0, E_2^0, I_2^0, B^0) - \mathbf{P}^*\| \leq \sigma,$$

we derive

$$\begin{aligned} E_1'(t) &\geq (\beta\lambda(t) + \beta_b(t)B(t))(S_1^* - \varrho) - \nu E_1(t) - \mu E_1(t), \\ I_1'(t) &\geq \nu E_1(t) - (\delta + \mu)I_1(t), \\ C'(t) &\geq \delta\theta I_1(t) + \delta\theta I_2(t) - \mu C(t), \\ E_2'(t) &\geq (\beta\lambda(t) + \beta_b(t)B(t))(S_2^* - \varrho) - \nu E_2(t) - \mu E_2(t), \\ I_2'(t) &\geq \nu E_2(t) - (\delta + \mu)I_2(t), \\ B'(t) &\geq \gamma\lambda(t) - \zeta B(t). \end{aligned}$$

Consider the system given below, which is used as an auxiliary system,

$$\begin{aligned} E_1'(t) &= (\beta\lambda(t) + \beta_b(t)B(t))(S_1^* - \varrho) - \nu E_1(t) - \mu E_1(t), \\ I_1'(t) &= \nu E_1(t) - (\delta + \mu)I_1(t), \\ C'(t) &= \delta\theta I_1(t) + \delta\theta I_2(t) - \mu C(t), \\ E_2'(t) &= (\beta\lambda(t) + \beta_b(t)B(t))(S_2^* - \varrho) - \nu E_2(t) - \mu E_2(t), \\ I_2'(t) &= \nu E_2(t) - (\delta + \mu)I_2(t), \\ B'(t) &= \gamma\lambda(t) - \zeta B(t). \end{aligned}$$

We can now conclude from the previous discussion that $\rho(\Phi_{\mathcal{F}-\nu-M_0}(T)) > 1$. By Lemma 1, there exists a function $p(t) > 0$, periodic with period T and it satisfies $p(t) \exp(\zeta t)$ as a solution of (5), where $\zeta = \frac{1}{T} \ln \rho(\Phi_{\mathcal{F}-\nu-M_0}(T)) > 0$. Considering each $G(0) \in \mathbb{R}_+^6$, there exists $K^* \in \mathbb{R}_+$ such that $G(0) \geq K^* p(0)$, where $G(t) = (E_1(t), I_1(t), C(t), E_2(t), I_2(t), B(t))^T$, and by ([34], Theorem B.1), we have $G(t) \geq p(t) \exp(\zeta t)$ for all $t > 0$. Therefore, it follows that $\lim_{t \rightarrow \infty} E_1(t) = \infty$, $\lim_{t \rightarrow \infty} I_1(t) = \infty$, $\lim_{t \rightarrow \infty} C(t) = \infty$, $\lim_{t \rightarrow \infty} E_2(t) = \infty$, $\lim_{t \rightarrow \infty} I_2(t) = \infty$, and $\lim_{t \rightarrow \infty} B(t) = \infty$, leading to a contradiction to $E_1(t) < \varrho$, $I_1(t) < \varrho$, $C(t) < \varrho$, $E_2(t) < \varrho$, $I_2(t) < \varrho$, $B(t) < \varrho$ and Equation (18). Hence, we have established the validity of Equation (17), which concludes the proof. \square

Theorem 5. Suppose that $\mathcal{R}_0 > 1$. In that case, system (1) admits at least a single positive periodic solution and there is a positive value ε such that

$$\begin{aligned} \liminf_{t \rightarrow \infty} E_1(t) &\geq \varepsilon, & \liminf_{t \rightarrow \infty} I_1(t) &\geq \varepsilon, & \liminf_{t \rightarrow \infty} R(t) &\geq \varepsilon, & \liminf_{t \rightarrow \infty} C(t) &\geq \varepsilon, \\ \liminf_{t \rightarrow \infty} E_2(t) &\geq \varepsilon, & \liminf_{t \rightarrow \infty} I_2(t) &\geq \varepsilon, & \liminf_{t \rightarrow \infty} B(t) &\geq \varepsilon, \end{aligned}$$

for all $(S_1^0, E_1^0, I_1^0, R^0, C^0, S_2^0, E_2^0, I_2^0, B^0) \in X_0$.

Proof. We aim to to establish the uniform persistence of \mathcal{P} regarding $(X_0, \partial X_0)$, which would imply that the solution of (1) is also uniformly persistent with respect to $(X_0, \partial X_0)$ by applying ([35], Theorem 3.1.1). To begin, we need to show that ∂X_0 and X_0 remain positively invariant under system (1). Given $(S_1^0, E_1^0, I_1^0, R^0, C^0, S_2^0, E_2^0, I_2^0, B^0) \in X_0$, we can solve (1) for all $t > 0$ to obtain

$$S_1(t) = \left[S_1^0 + \int_0^t (\Lambda + \eta S_2(s)) e^{\int_0^s (a(r)+\mu) dr} ds \right] e^{\int_0^t -(a(r)+\mu) dr} > 0, \tag{19}$$

$$E_1(t) = \left[E_1^0 + \int_0^t a(s)S_1(s)e^{(v+\mu)s} ds \right] e^{-(v+\mu)t} > 0, \tag{20}$$

$$I_1(t) = \left[I_1^0 + v \int_0^t E_1(s)e^{(\delta+\mu)s} ds \right] e^{-(\delta+\mu)t} > 0, \tag{21}$$

$$R(t) = \left[R^0 + \int_0^t \delta((1 - \alpha - \theta)I_1(s) + (1 - \theta)I_2(s))e^{(\omega+\mu)s} ds \right] e^{-(\omega+\mu)t} > 0, \tag{22}$$

$$C(t) = \left[C^0 + \int_0^t \delta\theta(I_1(s) + I_2(s))e^{\mu s} ds \right] e^{-\mu t} > 0, \tag{23}$$

$$S_2(t) = \left[S_2^0 + \int_0^t (\omega R(s))e^{\int_0^s (a(r)+\eta+\mu) dr} ds \right] e^{\int_0^t -(a(r)+\eta+\mu) dr} > 0, \tag{24}$$

$$E_2(t) = \left[E_2^0 + \int_0^t a(s)S_2(s)e^{(v+\mu)s} ds \right] e^{-(v+\mu)t} > 0, \tag{25}$$

$$I_2(t) = \left[I_2^0 + v \int_0^t E_2(s)e^{(\delta+\mu)s} ds \right] e^{-(\delta+\mu)t} > 0, \tag{26}$$

$$B(t) = \left[B^0 + \int_0^t \gamma\lambda(s)e^{\xi s} ds \right] e^{-\xi t} > 0, \tag{27}$$

where $a(t) = \beta\lambda(t) + \beta_b(t)B(t)$. Therefore, we established the positive invariance of X_0 under the dynamics of (1). Moreover, since ∂X_0 is relatively closed in X , it follows that ∂X_0 is also positively invariant and system (1) is point dissipative. Introducing

$$M_{\partial} = \left\{ (S_1^0, E_1^0, I_1^0, R^0, C^0, S_2^0, E_2^0, I_2^0, B^0) \in \partial X_0 : \right. \\ \left. P^m(S_1^0, E_1^0, I_1^0, R^0, C^0, S_2^0, E_2^0, I_2^0, B^0) \in \partial X_0, \forall m \geq 0 \right\}.$$

To establish our result, we will employ the uniform persistence theory as outlined in [35]. To do so, we need to demonstrate that $M_{\partial} = \mathcal{M}_{\partial}$, where \mathcal{M}_{∂} is given by

$$\mathcal{M}_{\partial} = \left\{ (S_1^0, E_1^0, I_1^0, R^0, C^0, S_2^0, E_2^0, I_2^0, B^0) \in \partial X_0 : \right. \\ \left. E_1^0 = I_1^0 = R^0 = C^0 = S_2^0 = E_2^0 = I_2^0 = B^0 = 0 \right\}.$$

We can observe that $M_{\partial} \supseteq \mathcal{M}_{\partial}$. To complete the proof, it suffices to demonstrate that $M_{\partial} \subset \mathcal{M}_{\partial}$. That is, for any initial value $(S_1^0, E_1^0, I_1^0, R^0, C^0, S_2^0, E_2^0, I_2^0, B^0) \in \partial X_0$, at least one of the following holds: $E_1(nT) = 0, I_1(nT) = 0, R(nT) = 0, C(nT) = 0, E_2(nT) = 0, I_2(nT) = 0$, or $B(nT) = 0$, for any $n \geq 0$.

Assuming the opposite, let there be a non-negative integer n_1 such that $E_1(n_1T), I_1(n_1T), R(n_1T), C(n_1T), E_2(n_1T), I_2(n_1T), B(n_1T)$ are all positive. By substituting $t = n_1T$ in Equations (19)–(27), we derive that $0 < S_1(t), 0 < E_1(t), 0 < I_1(t), 0 < R(t), 0 < C(t), 0 < S_2(t), 0 < E_2(t), 0 < I_2(t), 0 < B(t)$. This statement conflicts with the established truth that ∂X_0 is positively invariant.

Using Lemma 2 under the condition $\mathcal{R}_0 > 1$, we have established the weak uniform persistence of \mathcal{P} with respect to $(X_0, \partial X_0)$. Then we can conclude that \mathcal{P} has a global attractor by Proposition 1, and \mathbf{P}^* is an isolated invariant subset of X with $W^s(\mathbf{P}^*) \cap X_0 = \emptyset$. Furthermore, every solution in M_{∂} approaches \mathbf{P}^* , and \mathbf{P}^* is acyclic in M_{∂} . By ([35], Theorem 1.3.1, Remark 1.3.1), we can conclude that \mathcal{P} is uniform persistence with respect to $(X_0, \partial X_0)$. Therefore, there exists $\varepsilon > 0$ such that

$$\liminf_{t \rightarrow \infty} E_1(t) \geq \varepsilon, \quad \liminf_{t \rightarrow \infty} I_1(t) \geq \varepsilon, \quad \liminf_{t \rightarrow \infty} R(t) \geq \varepsilon, \quad \liminf_{t \rightarrow \infty} C(t) \geq \varepsilon, \\ \liminf_{t \rightarrow \infty} E_2(t) \geq \varepsilon, \quad \liminf_{t \rightarrow \infty} I_2(t) \geq \varepsilon, \quad \liminf_{t \rightarrow \infty} B(t) \geq \varepsilon.$$

According to ([35], Theorem 1.3.6), there exists $\tilde{\phi} \in X_0$ as an equilibrium for \mathcal{P} , which implies the existence of a minimum of single periodic solution $u(t, \tilde{\phi})$ for (1). Here, $\tilde{\phi}$ is

given by $\tilde{\varphi} = (\tilde{S}_1(0), \tilde{E}_1(0), \tilde{I}_1(0), \tilde{R}(0), \tilde{C}(0), \tilde{S}_2(0), \tilde{E}_2(0), \tilde{I}_2(0), \tilde{B}(0)) \in X_0$. To show that $\tilde{S}_1(0)$ and $\tilde{S}_2(0)$ are positive, suppose otherwise, i.e., $\tilde{S}_1(0) = \tilde{S}_2(0) = 0$. Then, by the periodicity of u for all $n \geq 0$, we have $\tilde{S}_1(nT) = \tilde{S}_2(nT) = 0$. However, this leads to a contradiction as it violates the positive invariance of X_0 . Hence, $\tilde{S}_1(0) > 0$ and $\tilde{S}_2(0) > 0$ for all $t > 0$. \square

5. Numerical Simulations

This section is dedicated to presenting numerical simulations that aim to illustrate and validate the theoretical findings discussed in the preceding sections. These simulations provide visual evidence of the alignment between our periodic model (1) and the observed seasonal variations. Following [22], we assume that

$$\beta_b(t) = \bar{\beta}_b \left(1 + \Pi \cos\left(\frac{2\pi t - \varphi}{52}\right) \right),$$

where $\bar{\beta}_b$ is the baseline long-period transmission rate, Π is the amplitude of seasonal forcing, and φ is the seasonal offset parameter.

5.1. Extinction and Persistence

As mentioned in Section 4, the BRNP \mathcal{R}_0 plays a critical role as a threshold parameter in determining the extinction and persistence of TyF within the population. Theorems 3 to 5 provide further insights into this relationship. The numerical results presented in Figures 2 and 3 provide clear evidence that the solutions obtained from our model (1), with initial values set as $S_1^0 = 2000, E_1^0 = 200, I_1^0 = 30, R^0 = 100, C^0 = 20, S_2^0 = 2000, E_2^0 = 100, I_2^0 = 15$, and $B^0 = 4000$, are consistent with the analytical findings. These findings establish that the single DFPS \mathbf{P}^* maintains GAS under the condition $\mathcal{R}_0 \approx 0.8933 < 1$ and the disease goes extinct.

Figures 4–6 provide visual representations of the prolonged dynamics and consistent persistence of the disease when $\mathcal{R}_0 \approx 15.55 > 1$. This high value indicates that the disease compartments persist, leading to an endemic state within the population, with annual recurrences of the epidemic. The graphs effectively demonstrate the long-term behavior and uniform persistence of TyF over time. For a comprehensive understanding of the parameter values, ranges, and units employed in both cases, please refer to Table 2 and the initial values set as $S_1^0 = 35,000, E_1^0 = 100, I_1^0 = 80, R^0 = 500, C^0 = 20, S_2^0 = 2000, E_2^0 = 50, I_2^0 = 40$, and $B^0 = 10,000$. The figures depict both the periodic model and its autonomous version. As observed in Figures 4 and 5, the disease persists in both cases due to the parameter settings used. In the context of the non-autonomous model, it is important to emphasize that periodic solutions are present.

Table 2. Parameters, values, ranges, and units for model (1).

Parameters	Values Extinction	Values Persistence	Range	Unites	Source
Λ	500	140	100–1000	Week	[36]
μ	0.00027	0.0007	$(2.30\text{--}3.60) \times 10^{-4}$	Week	[37]
β	1×10^{-10}	1×10^{-7}	0–0.1	Week	[18,22]
τ	0.05	0.196	0–0.2	Week	[18,22]
$\bar{\beta}_b$	1×10^{-11}	8×10^{-8}	0–0.1	Week	[18,22]
Π	0.544	0.7696	0–1	–	[18,22]
φ	4.37	5.41	1–10	–	[18,22]
γ	1	1.634	0–2	Week	[18,22]
ν	0.102	0.112	0–1	Week	[8,38]
θ	0.0292	0.0453	0.003–0.1	–	[28]
δ	0.143	0.432	0–1	Week	[8]
α	0.0025	0.188	0.001–0.2	Week	[39,40]
ω	0.0054	0.0054	$6.66 \times 10^{-3}\text{--}0.0125$	Week	[8]
η	0.000083	0.000083	0–0.01	Week	[18,22]
ξ	0.217	0.26	0.001–0.5	Week	[41]

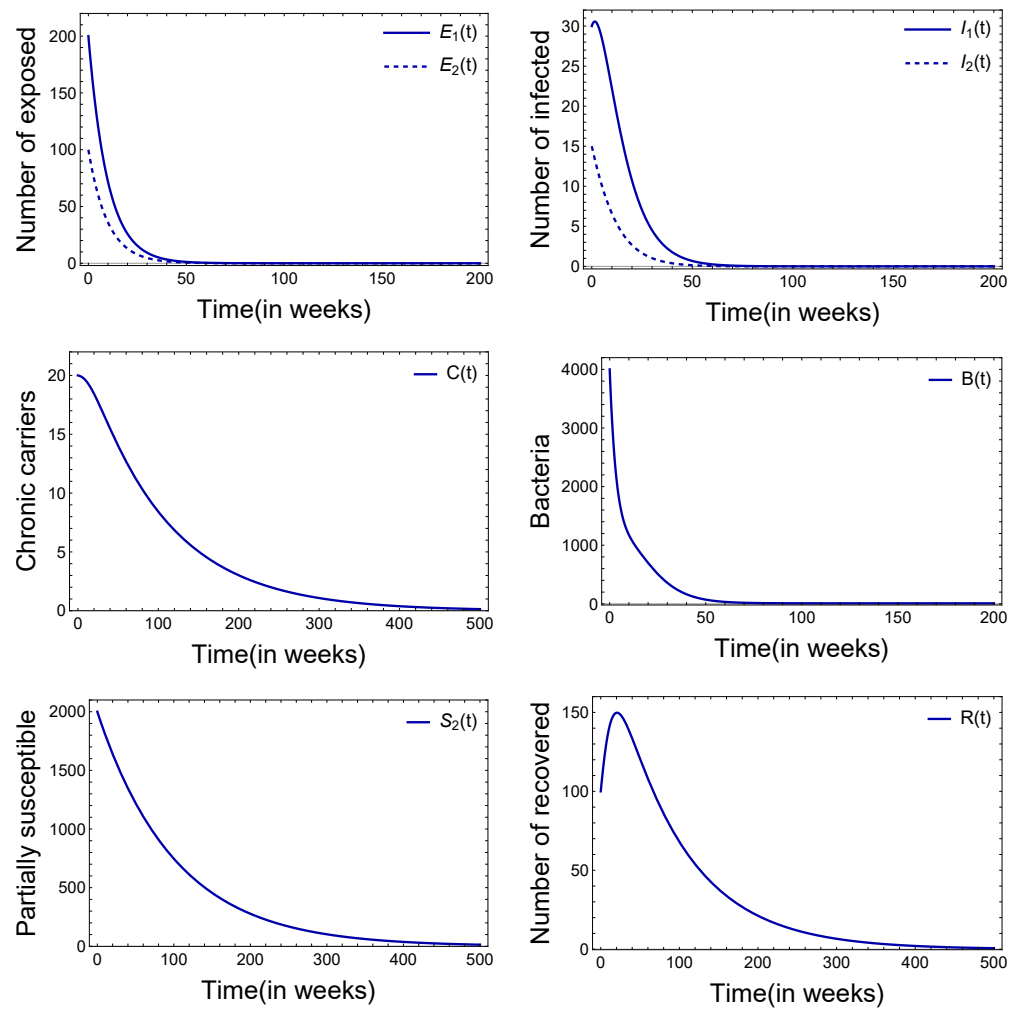


Figure 2. Extinction of typhoid when $\mathcal{R}_0 = 0.8933 < 1$, given the specific parameter values specified in Table 2 (extinction).

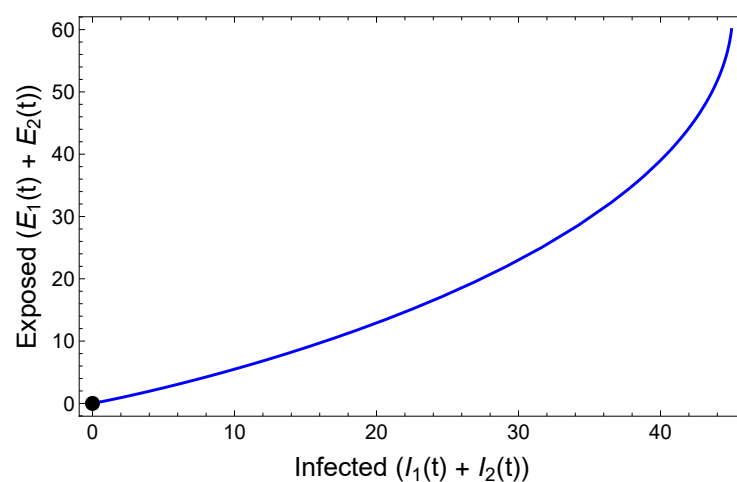


Figure 3. GAS of P^* when $\mathcal{R}_0 = 0.8933 < 1$, given the specific parameter values specified in Table 2 (extinction).

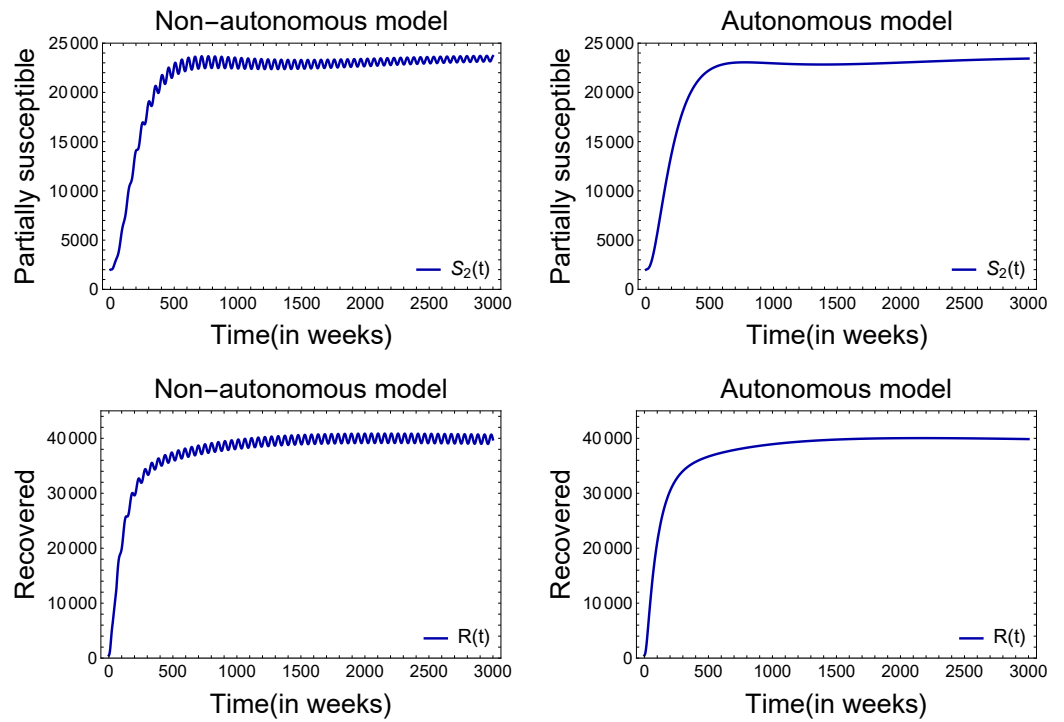


Figure 4. Persistence of typhoid when $\mathcal{R}_0 = 15.55 > 1$, given the specific parameter values specified in Table 2 (persistence).

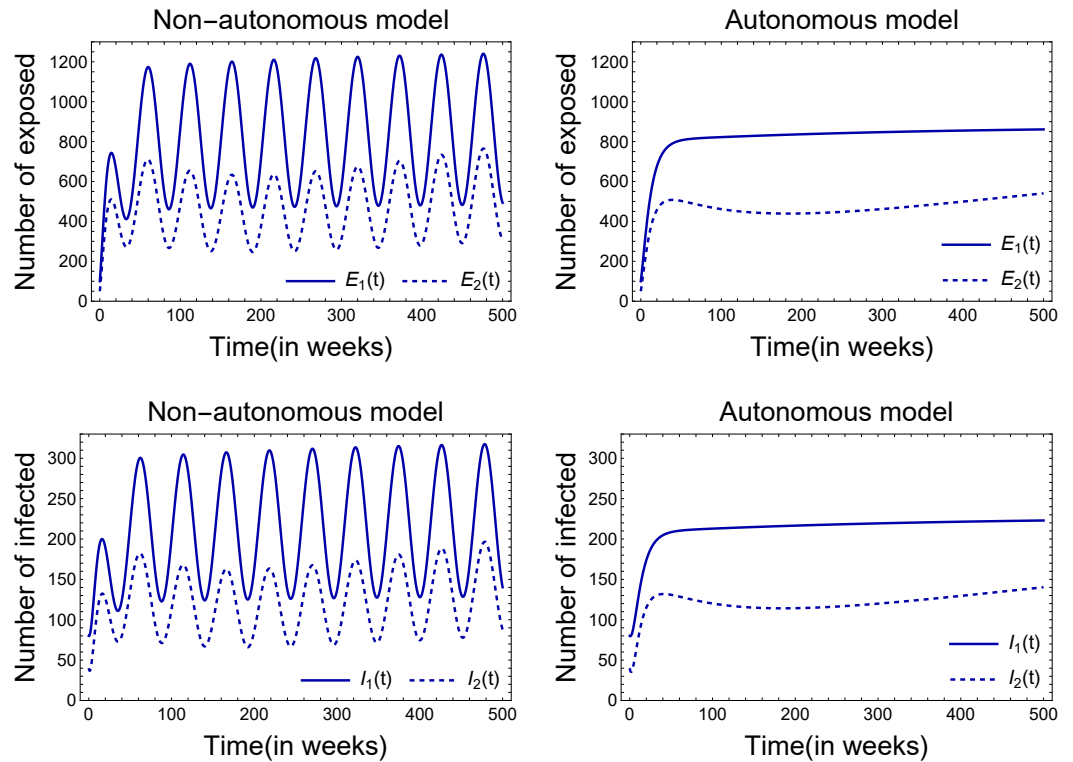


Figure 5. Cont.

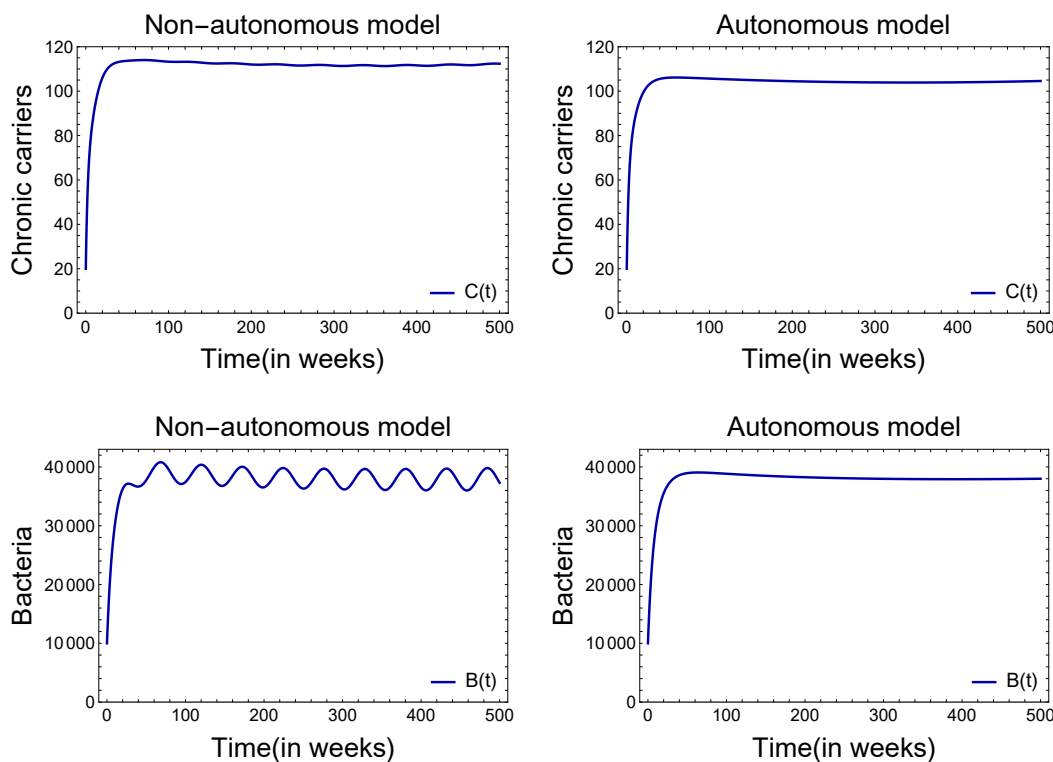


Figure 5. Persistence of typhoid when $\mathcal{R}_0 = 15.55 > 1$, given the specific parameter values specified in Table 2 (persistence).

This means that the disease exhibits recurrent patterns and fluctuations over time, adding an additional dynamic element to its persistence.

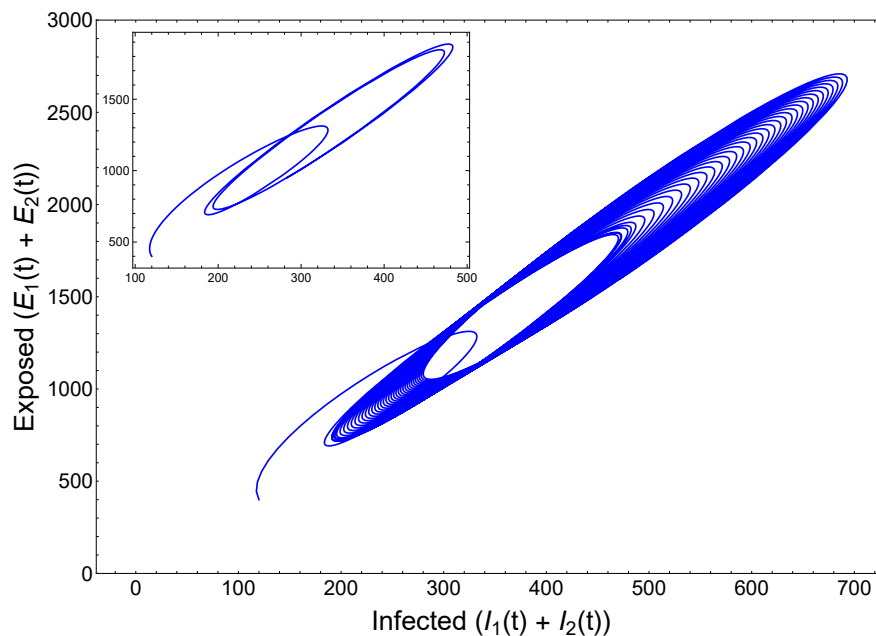


Figure 6. Positive periodic solutions when $\mathcal{R}_0 = 15.55 > 1$, given the specific parameter values specified in Table 2 (persistence).

5.2. Sensitivity Analysis

Sensitivity analysis refers to the study of how uncertainties in a model’s parameters can be attributed to various sources of uncertainty in its parameters [42]. In order to

identify influential parameters and evaluate their impact on output variability, it is crucial to conduct a sensitivity analysis that focuses explicitly on the parameters associated with the system. Sensitivity indices offer a way to measure the proportional impact of parameter variations on a state variable. The normalized forward sensitivity index measures this influence for a variable x that is differentiable with respect to a parameter p . It is determined by comparing the relative changes in x and p , and can be mathematically expressed as follows [43]:

$$\Psi_p^x = \frac{\partial x}{\partial p} \times \frac{p}{x}.$$

We first conduct a sensitivity analysis for the BRNA \mathcal{R}_0^A given in (10) and the BRNT $[\mathcal{R}_0]$ given in (11). To perform the sensitivity analysis, specific parameter values were chosen, which are presented in Table 2. The sensitivity indices for \mathcal{R}_0^A , $[\mathcal{R}_0]$, \mathcal{R}_{0h} , and \mathcal{R}_{0b} are provided in Table 3. According to the data provided in Table 3, reducing the values of β , τ , θ , $\bar{\beta}_b$, and γ by 10% leads to a decrease in $[\mathcal{R}_0]$ by approximately 5.8%, 4.3%, 4.3%, 4.16%, and 4.16%, respectively. Conversely, increasing the values of μ , α , and ξ by 10% results in a decrease in $[\mathcal{R}_0]$ by approximately 8.69%, 5.69%, and 3.15%, respectively. Similar results are obtained for \mathcal{R}_0^A .

The findings presented in Figure 7a,b demonstrate that the BRNA \mathcal{R}_0^A and the BRNT $[\mathcal{R}_0]$ are most sensitive to the natural mortality rate (μ), human-to-human infection rate (β), disease-induced mortality (α), followed equally by fraction infected who become chronic carriers (θ) and relative infectiousness of chronic carriers (τ). The least influenced for \mathcal{R}_0^A and $[\mathcal{R}_0]$ are the environment to human infection rate ($\bar{\beta}_b$), bacteria excretion (γ), bacterial decay rate (ξ), and 1/the duration of infectiousness (δ). While \mathcal{R}_{0h} is most influenced by β , μ , α , θ , τ , and δ , \mathcal{R}_{0b} is most sensitive to $\bar{\beta}_b$, γ , ξ , μ , α , τ , and δ (see Figure 7c,d).

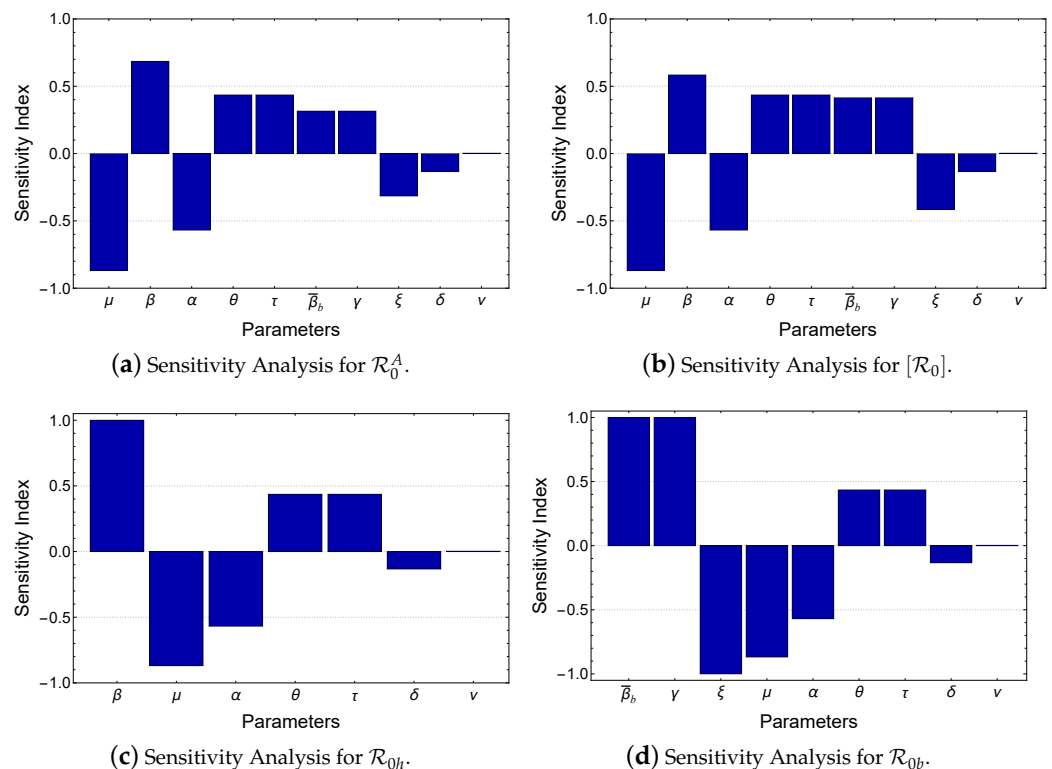


Figure 7. Sensitivity analysis for \mathcal{R}_0^A , $[\mathcal{R}_0]$, \mathcal{R}_{0h} , and \mathcal{R}_{0b} , given the specific parameter values specified in Table 2. Sensitivity indices are arranged in descending order of magnitude.

Table 3. Sensitivity indices of \mathcal{R}_0^A , $[\mathcal{R}_0]$, \mathcal{R}_{0h} , and \mathcal{R}_{0b} to parameters in model (1), assessed by utilizing the baseline parameter values listed in Table 2.

Parameter	Sensitivity Index \mathcal{R}_0^A	Sensitivity Index $[\mathcal{R}_0]$	Sensitivity Index \mathcal{R}_{0h}	Sensitivity Index \mathcal{R}_{0b}
μ	−0.868986	−0.868986	−0.868986	−0.868986
β	+0.684542	+0.584275	+1	−
α	−0.569721	−0.569721	−0.569721	−0.569721
θ	+0.436067	+0.436067	+0.436067	+0.436067
τ	+0.436067	+0.436067	+0.436067	+0.436067
$\bar{\beta}_b$	+0.315458	+0.415725	−	+1
γ	+0.315458	+0.415725	−	+1
ξ	−0.315458	−0.415725	−	−1
δ	−0.133654	−0.133654	−0.133654	−0.133654
ν	+0.00264	+0.00264	+0.00264	+0.00264

It is crucial to understand the numerous parameters that influence the Model (1) variables. By using eFAST in the MATLAB software (see [44] for more details), the parameter sensitivity analysis for the infected classes is performed. In eFAST, sensitivity indices are computed while simultaneously modifying all parameters within predetermined limits. The magnitude of the derived sensitivity indices determines the significance of the parameters on the outcomes of the model’s variability [44,45]. All parameters fluctuate according to the precise ranges and benchmark values specified in Table 2, and the baseline values are (Values Persistence), assuming uniform distributions. The sensitivity indices for the model variable are determined at one year. Calculated and displayed in Figure 8a,b, respectively, are the sensitivity indices for I_1 and I_2 . The number of infected humans is influenced by various factors, as shown in Figure 8. Higher transmission parameters, such as β , $\bar{\beta}_b$, γ , and τ , lead to an increase in the number of infected individuals. On the other hand, an increase in the bacterial decay rate ξ , as well as the immunity parameters η and ω , results in a decrease in the number of infected individuals.

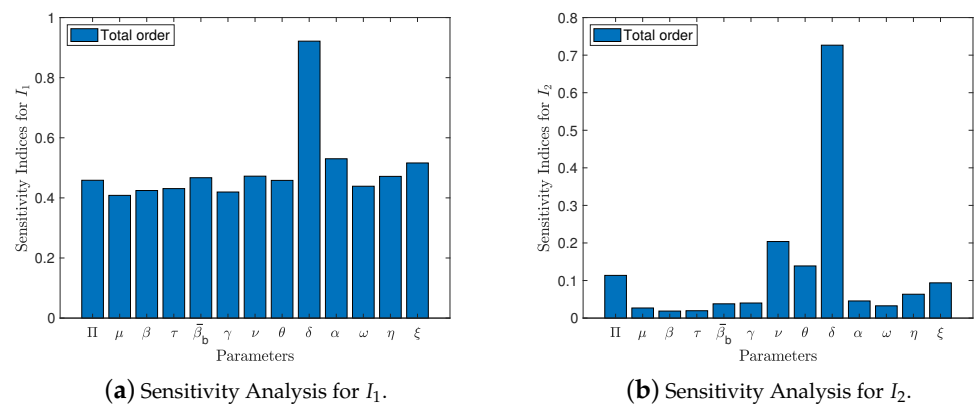


Figure 8. Model (1) sensitivity analysis output, using the parameter values specified in Table 2.

Then, in Figures 9 and 10, we numerically display \mathcal{R}_0^A of the autonomous model and $[\mathcal{R}_0]$ of the related model that changes over time depends on the parameters that have the most impact. (β , $\bar{\beta}_b$, γ , τ , θ , δ , ξ , and μ). The results show that \mathcal{R}_0^A is less than $[\mathcal{R}_0]$ indicating that \mathcal{R}_0^A gives a low estimate of how likely it is that an infection will spread. Remarkably, our findings align with those reported in [23,25,46], where they present diverse outcomes concerning the underestimation and overestimation of $[\mathcal{R}_0]$. In [23], their findings showed that $[\mathcal{R}_0]$ gives a lower estimate of the risk of malaria spread.

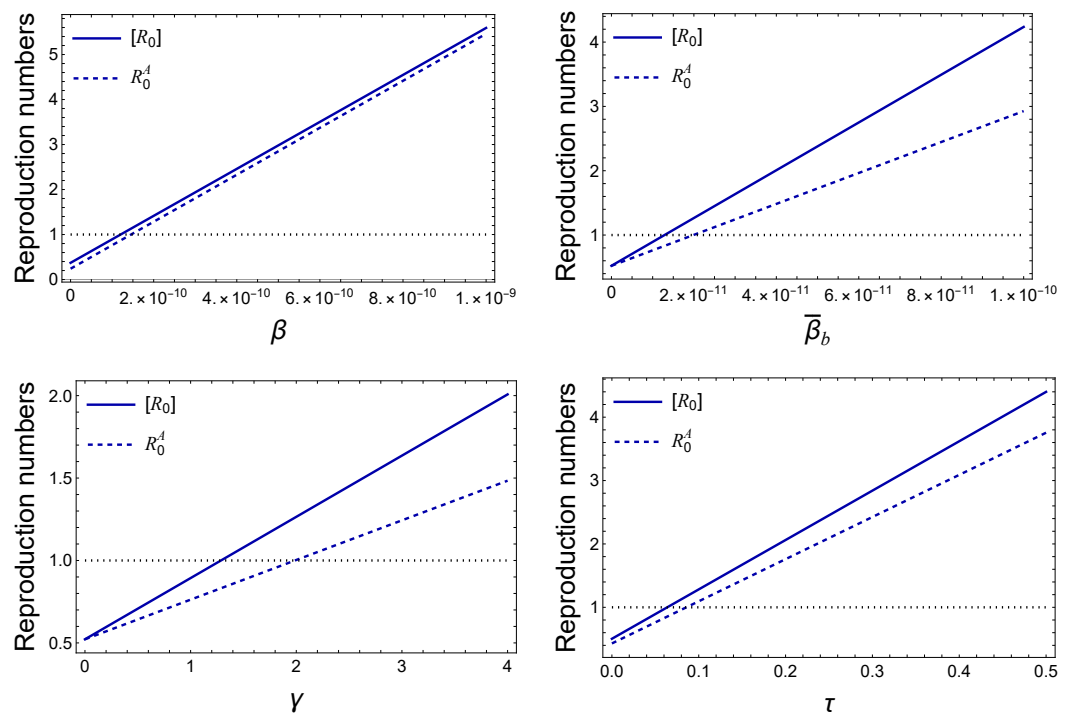


Figure 9. Sensitivity of the reproduction numbers \mathcal{R}_0^A and $[\mathcal{R}_0]$ with respect to the Model (1) parameters, given the specific parameter values specified in Table 2.

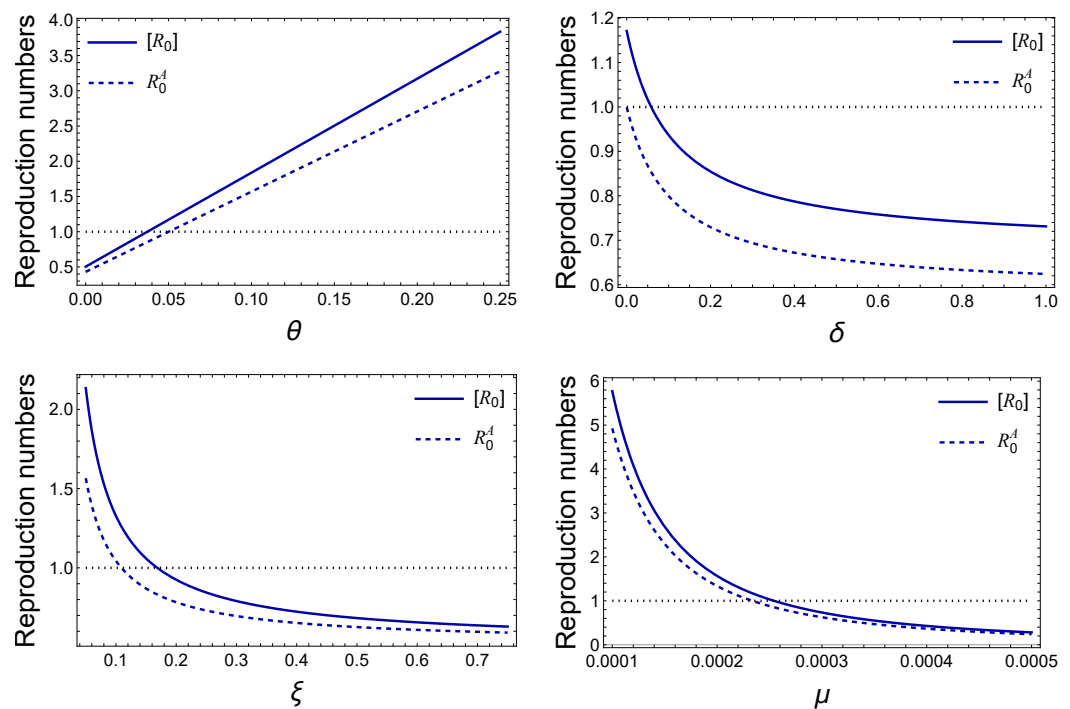


Figure 10. Sensitivity of the reproduction numbers \mathcal{R}_0^A and $[\mathcal{R}_0]$ with respect to the Model (1) parameters, given the specific parameter values specified in Table 2.

5.3. Effects of Parameter Modifications and Control

Modifying Model (1) parameters plays a crucial role in understanding the dynamics of TyF transmission and formulating effective control strategies. The sensitivity analysis conducted in the study provides insights into how different parameters influence the reproduction numbers (\mathcal{R}_0 , $[\mathcal{R}_0]$, and \mathcal{R}_0^A) as well as the number of human infections (I_1 and I_2) and, consequently, the spread of TyF. By comprehending the effects of parameter

modifications, we can identify key factors that contribute to the transmission of TyF and devise targeted control measures. Here, we discuss some significant parameters and their implications in implementing efficient control strategies to combat TyF through a series of numerical simulations. We assume that the disease is persisting in the population as well as that the number of chronic cases is high with an initial infection of approximately 20,000 cases.

Figure 11 shows the rate at which infected individuals transmit TyF to susceptible ones due to short or long transmission periods (β and $\bar{\beta}_b$). Increasing either of these rates leads to higher human infection (I_1 and I_2). In particular, the baseline environment-to-human infection rate ($\bar{\beta}_b$) significantly impacts the number of infections, and even if β is equal to zero, we observe that the disease persists as studied in [20]. This indicates that TyF can spread via indirect or long-period transmission only, and control efforts should focus not only on prioritizing social distancing, isolating infected individuals, and promoting hygienic practices to reduce contact and interactions between infected and susceptible individuals, but also on additional strategies targeting environmental contamination through ensuring clean water supplies, proper waste disposal, and improved hygiene practices to curb transmission.

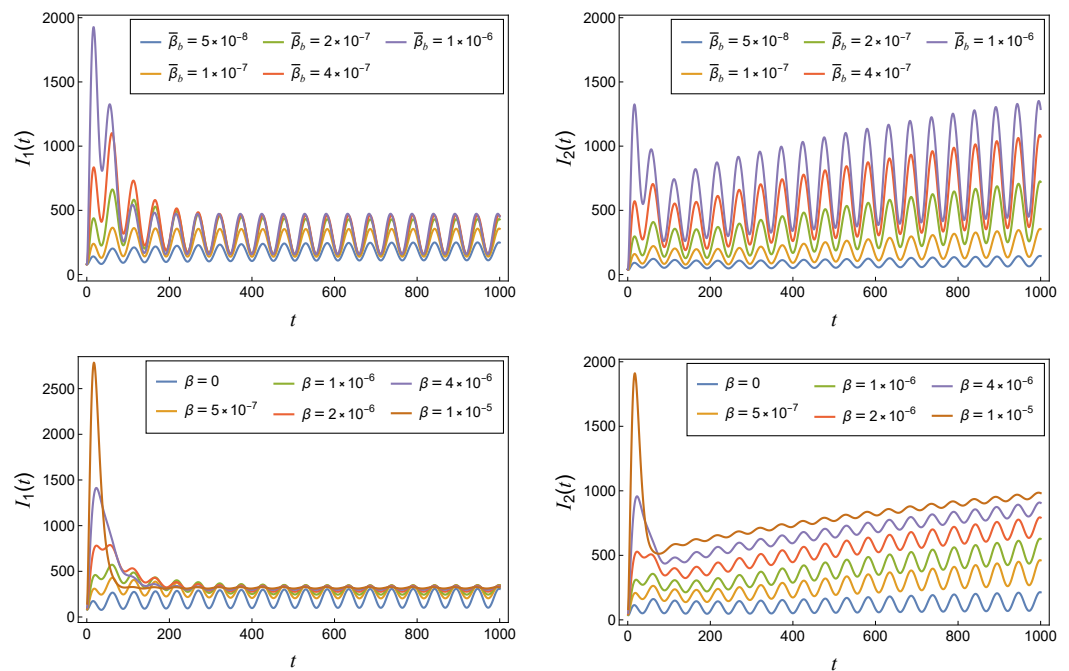


Figure 11. Solutions (I_1 and I_2) of Model (1) plotted with respect to the parameters β and $\bar{\beta}_b$, given the specific parameter values specified in Table 2 (persistence).

As seen in Figure 12, the number of infected humans (I_1 and I_2) is plotted against the proportion of infected individuals who transition into chronic carriers (θ) and the relative infectiousness of chronic carriers (τ). Higher values of θ and τ indicate the significance of chronic carriers in typhoid fever transmission. Reducing the proportion of infected individuals transitioning into chronic carriers (higher θ) and minimizing the infectiousness of chronic carriers (higher τ) through targeted interventions like regular screening and timely treatment of acute infections is crucial for controlling the disease.

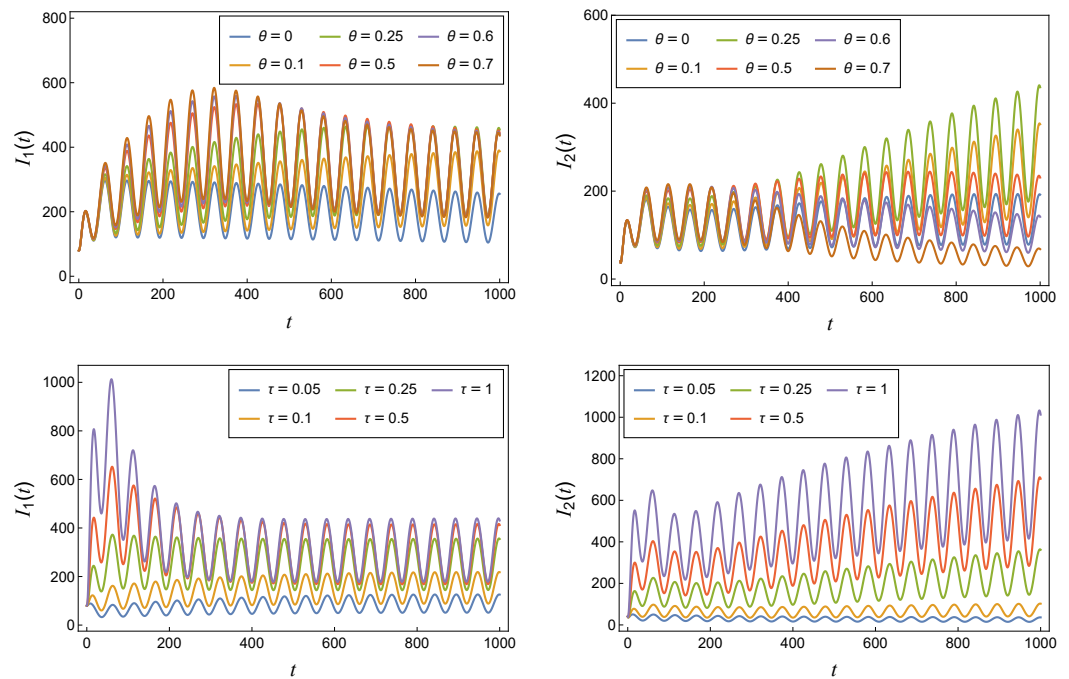


Figure 12. Solutions (I_1 and I_2) of Model (1) plotted with respect to the parameters θ and τ , given the specific parameter values specified in Table 2 (persistence).

The significant impact of the bacterial excretion rate (γ) and the bacterial decay rate (ξ) on long-period infections is demonstrated in Figure 13. Higher values of γ correspond to increased I_1 and I_2 , indicating a higher likelihood of long-lasting infection periods. Additionally, ξ exhibits an inverse relationship with the number of infected individuals. A higher value of ξ results in a lower incidence of infection. These findings suggest that interventions focused on targeting bacterial decay can play a crucial role in controlling TyF.

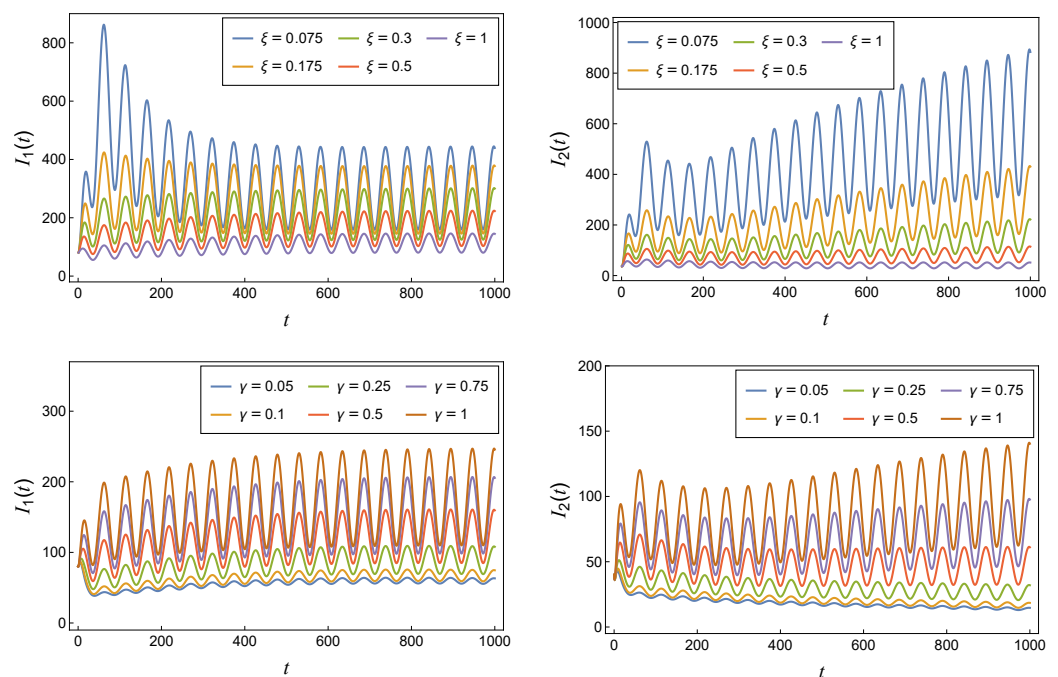


Figure 13. Solutions (I_1 and I_2) of Model (1) plotted with respect to the parameters ξ and γ , given the specific parameter values specified in Table 2 (persistence).

Modifying model parameters and understanding their influence on TyF transmission are crucial for formulating effective control strategies. Targeting chronic carriers, reducing infection rates through interventions like screening and treatment, and implementing hygiene and environmental control measures are essential steps in curbing TyF spread.

6. Discussion

The utilization of mathematical models is essential for predicting the dynamics of diseases and estimating critical quantities. One of the advantages of non-autonomous models like ours is their ability to capture temporal variations and changes in the system. This study aimed to analyze TyF transmission in a population through a compartmental model, considering the dynamic changes occurring periodically in the environment.

Firstly, we calculate the BRNP, \mathcal{R}_0 , for the periodic model. Furthermore, we derive an expression for the BRNT, $[\mathcal{R}_0]$, for the non-autonomous model, and the BRNA, \mathcal{R}_0^A , for the autonomous model. An analysis was conducted to examine the GAS of \mathbf{P}^* and endemic periodic solutions. It has been shown that when $\mathcal{R}_0 < 1$, \mathbf{P}^* is globally asymptotic stable, indicating TyF goes extinct. Conversely, when $\mathcal{R}_0 > 1$, the disease spreads through the population (see Theorem 4), which proves that there is a positive cyclical solution (refer to Theorem 5). Furthermore, the numerical simulations following the theoretical results were shown in this study (see Figures 2–6).

The sensitivity analysis of \mathcal{R}_0^A , for the constant version of the model, as well as $[\mathcal{R}_0]$, for the seasonal system described by 1, was conducted. The analysis aimed to assess the impact of the model's parameters on these quantities. The results suggested that the human-to-human infection rate (β) is an essential element in \mathcal{R}_0^A and the influence of β on the comparison between \mathcal{R}_0^A and $[\mathcal{R}_0]$ is negligible (see Figures 7a,b, 9 and 10). Simultaneously, the environment-to-human infection rate ($\bar{\beta}_b$) and bacteria excretion (γ) are also critical in reducing the basic reproduction number for long-cycle infections, \mathcal{R}_{0b} , and the influence of $\bar{\beta}_b$ and γ on the comparison between \mathcal{R}_0^A and $[\mathcal{R}_0]$ is significant (see Figures 7d, 9 and 10). As noted, $[\mathcal{R}_0]$ is greater than or equal to \mathcal{R}_0^A (see Figures 9 and 10). Therefore, $[\mathcal{R}_0]$ presents an overestimation of the threat of disease spread, whereas \mathcal{R}_0^A underestimates the level of potential infection. The model's sensitivity indices for the variable are calculated at a one-year interval. The infected individuals by TyF are impacted by multiple factors (see Figure 8). Elevated transmission parameters, such as β , $\bar{\beta}_b$, γ , and τ , are associated with an increased incidence of infection. Conversely, a higher bacterial decay rate, represented by ζ , as well as increased immunity parameters η and ω are linked to a reduced number of infected individuals.

The numerical simulations presented in Figure 11 through Figure 13 highlight the significance of chronic carriers in TyF transmission. Reducing the transition proportion (θ) and infectiousness (τ) of chronic carriers through screening and timely treatment is crucial for control. The analysis reveals the impact of bacterial excretion rate (γ) and decay rate (ζ) on long-lasting infections. Higher γ increases infection rates, while higher ζ reduces the number of infections. Targeting bacterial decay is essential for effective TyF control.

Preventing transmission is paramount to avoiding TyF. Food and water contamination are the primary vectors for disease transmission, highlighting the significance of practicing good hygiene. Vaccination is also crucial in protecting against TyF. Additionally, efforts must be directed toward controlling bacterial contamination by implementing strategies for safe water supplies, sanitation, and hygiene practices. Lastly, prioritizing immune system health is essential for overall well-being.

One of the limitations of our model is that limited knowledge exists regarding parameter values, which limits its quantitative accuracy. However, the qualitative results remain consistent even when considering alternative parameter values. There are numerous potential avenues for further development of our model. As stated earlier, different regions may experience distinct seasonal patterns that affect the incidence and spread of TyF; therefore, a model that includes periodic parameters for human-to-human infection could be developed. Additional promising future research directions for understanding TyF transmission

dynamics involve extending the current ordinary differential equation model to incorporate partial differential equations, capturing spatial variations in disease dynamics in diverse endemic regions. Furthermore, integrating a vaccination compartment for humans into the model can significantly impact disease transmission dynamics. By considering vaccination rates, coverage, and vaccine efficacy, we can explore the potential impact of vaccination campaigns on reducing transmission and controlling outbreaks. Additionally, calibrating and expanding the model specifically for typhoid-endemic regions like South Asia and Africa, by integrating region-specific characteristics and local epidemiological data, would enhance its predictive accuracy. The incorporation of these advancements in future research will significantly contribute to the study of typhoid fever dynamics and aid in devising more effective strategies for disease control.

Author Contributions: Conceptualization, F.K.A., M.H.A. and M.A.I.; methodology, F.K.A., M.H.A. and M.A.I.; software, F.K.A., M.H.A. and M.A.I.; validation, F.K.A., M.H.A. and M.A.I.; formal analysis, M.A.I.; investigation, F.K.A., M.H.A. and M.A.I.; writing—original draft preparation, F.K.A., M.H.A. and M.A.I.; writing—review and editing, F.K.A., M.H.A. and M.A.I.; visualization, F.K.A., M.H.A. and M.A.I.; funding acquisition, F.K.A. All authors have read and agreed to the published version of the manuscript.

Funding: This work was funded by the Najran University, Najran, Saudi Arabia, under grant code (NU/NRP/SERC/12/3).

Data Availability Statement: Not applicable.

Acknowledgments: The authors are thankful to the Deanship of Scientific Research at Najran University for funding this work under the Research Priorities and Najran Research funding program, grant code (NU/NRP/SERC/12/3). The authors are grateful to the anonymous reviewers and the scientific editor for their insightful and constructive comments and suggestions, which helped to improve the paper.

Conflicts of Interest: The authors declare no conflict of interest.

References

1. James, S.L.; Abate, D.; Abate, K.H.; Abay, S.M.; Abbafati, C.; Abbasi, N.; Abbastabar, H.; Abd-Allah, F.; Abdela, J.; Abdelalim, A.; et al. Global, regional, and national incidence, prevalence, and years lived with disability for 354 diseases and injuries for 195 countries and territories, 1990–2017: A systematic analysis for the Global Burden of Disease Study 2017. *Lancet* **2018**, *392*, 1789–1858. [[CrossRef](#)] [[PubMed](#)]
2. Crump, J.A.; Sjölund-Karlsson, M.; Gordon, M.A.; Parry, C.M. Epidemiology, clinical presentation, laboratory diagnosis, antimicrobial resistance, and antimicrobial management of invasive Salmonella infections. *Clin. Microbiol. Rev.* **2015**, *28*, 901–937. [[CrossRef](#)]
3. Centers for Disease Control and Prevention. Typhoid Fever and Paratyphoid Fever. Available online: <https://www.cdc.gov/typhoid-fever/index.html> (accessed on 1 June 2023).
4. World Health Organization. Typhoid. Available online: <https://www.who.int/news-room/fact-sheets/detail/typhoid> (accessed on 1 June 2023).
5. Mogasale, V.; Maskery, B.; Ochiai, R.L.; Lee, J.S.; Mogasale, V.V.; Ramani, E.; Kim, Y.E.; Park, J.K.; Wierzb, T.F. Burden of typhoid fever in low-income and middle-income countries: A systematic, literature-based update with risk-factor adjustment. *Lancet Glob. Health* **2014**, *2*, e570–e580. [[CrossRef](#)]
6. Shpargel, J.S.; Berardi, R.S.; Lenz, D. Salmonella typhi carrier state 52 years after illness with typhoid fever: A case study. *Am. J. Infect. Control* **1985**, *13*, 122–123. [[CrossRef](#)]
7. Sinnott, C.; Teall, A. Persistent gallbladder carriage of Salmonella typhi. *Lancet* **1987**, *329*, 976. [[CrossRef](#)]
8. Hornick, R.; Greisman, S.; Woodward, T.; DuPont, H.; Hawkins, A.; Snyder, M. Typhoid fever: Pathogenesis and immunologic control. *N. Engl. J. Med.* **1970**, *283*, 739–746. [[CrossRef](#)]
9. Glynn, J.; Hornick, R.; Levine, M.; Bradley, D. Infecting dose and severity of typhoid: Analysis of volunteer data and examination of the influence of the definition of illness used. *Epidemiol. Infect.* **1995**, *115*, 23–30. [[CrossRef](#)]
10. Mutua, J.M.; Wang, F.B.; Vaidya, N.K. Modeling malaria and typhoid fever co-infection dynamics. *Math. Biosci.* **2015**, *264*, 128–144. [[CrossRef](#)]
11. Tilahun, G.T.; Makinde, O.D.; Malonza, D. Co-dynamics of pneumonia and typhoid fever diseases with cost effective optimal control analysis. *Appl. Math. Comput.* **2018**, *316*, 438–459. [[CrossRef](#)]
12. Karunditu, J.W.; Kimathi, G.; Osman, S. Mathematical modeling of typhoid fever disease incorporating unprotected humans in the spread dynamics. *J. Adv. Math. Comput. Sci.* **2019**, *32*, 1–11. [[CrossRef](#)]

13. Chen, M.; Wu, R.; Zheng, Q. Nonconstant Steady States of a Rumor Propagation Model. *Differ. Equations Dyn. Syst.* **2023**, 1–29. [[CrossRef](#)]
14. Chen, M.; Hu, Z.; Zheng, Q.; Srivastava, H.M. Dynamics analysis of a spatiotemporal SI model. *Alex. Eng. J.* **2023**, *74*, 705–714. [[CrossRef](#)]
15. Chen, M.; Wu, R.; Zheng, Q. Qualitative analysis of a diffusive COVID-19 model with non-monotone incidence rate. *J. Appl. Anal. Comput.* **2023**, *13*, 2229–2249. [[CrossRef](#)] [[PubMed](#)]
16. Mushayabasa, S. A simple epidemiological model for typhoid with saturated incidence rate and treatment effect. *Int. J. Math. Comput. Sci.* **2013**, *6*, 688–695.
17. González-Guzmán, J. An epidemiological model for direct and indirect transmission of typhoid fever. *Math. Biosci.* **1989**, *96*, 33–46. [[CrossRef](#)] [[PubMed](#)]
18. Pitzer, V.E.; Bowles, C.C.; Baker, S.; Kang, G.; Balaji, V.; Farrar, J.J.; Grenfell, B.T. Predicting the impact of vaccination on the transmission dynamics of typhoid in South Asia: A mathematical modeling study. *PLoS Neglected Trop. Dis.* **2014**, *8*, e2642. [[CrossRef](#)]
19. Irena, T.K.; Gakkhar, S. Modelling the dynamics of antimicrobial-resistant typhoid infection with environmental transmission. *Appl. Math. Comput.* **2021**, *401*, 126081. [[CrossRef](#)]
20. Abboubakar, H.; Racke, R. Mathematical modeling, forecasting, and optimal control of typhoid fever transmission dynamics. *Chaos Solitons Fractals* **2021**, *149*, 111074. [[CrossRef](#)]
21. Matsebula, L.; Nyabadza, F.; Mushanyu, J. Mathematical analysis of typhoid fever transmission dynamics with seasonality and fear. *Commun. Math. Biol. Neurosci.* **2021**, *2021*, 36.
22. Pitzer, V.E.; Feasey, N.A.; Msefula, C.; Mallewa, J.; Kennedy, N.; Dube, Q.; Denis, B.; Gordon, M.A.; Heyderman, R.S. Mathematical modeling to assess the drivers of the recent emergence of typhoid fever in Blantyre, Malawi. *Clin. Infect. Dis.* **2015**, *61*, S251–S258. [[CrossRef](#)]
23. Ibrahim, M.A.; Dénes, A. Threshold and stability results in a periodic model for malaria transmission with partial immunity in humans. *Appl. Math. Comput.* **2021**, *392*, 125711. [[CrossRef](#)]
24. Rebelo, C.; Margheri, A.; Bacaër, N. Persistence in seasonally forced epidemiological models. *J. Math. Biol.* **2011**, *64*, 933–949. [[CrossRef](#)]
25. Wang, W.; Zhao, X.Q. Threshold dynamics for compartmental epidemic models in periodic environments. *J. Dyn. Differ. Equ.* **2008**, *20*, 699–717. [[CrossRef](#)]
26. Ibrahim, M.A.; Dénes, A. A mathematical model for Lassa fever transmission dynamics in a seasonal environment with a view to the 2017–20 epidemic in Nigeria. *Nonlinear Anal. Real World Appl.* **2021**, *60*, 103310. [[CrossRef](#)]
27. Ibrahim, M.A.; Dénes, A. Stability and Threshold Dynamics in a Seasonal Mathematical Model for Measles Outbreaks with Double-Dose Vaccination. *Mathematics* **2023**, *11*, 1791. [[CrossRef](#)]
28. Ames, W.R.; Robins, M. Age and sex as factors in the development of the typhoid carrier state, and a method for estimating carrier prevalence. *Am. J. Public Health Nations Health* **1943**, *33*, 221–230. [[CrossRef](#)] [[PubMed](#)]
29. Smith, H.L. *Monotone Dynamical Systems: An Introduction to the Theory of Competitive and Cooperative Systems: An Introduction to the Theory of Competitive and Cooperative Systems*; Number 41; American Mathematical Soc.: Providence, RI, USA, 1995.
30. Van den Driessche, P.; Watmough, J. Reproduction numbers and sub-threshold endemic equilibria for compartmental models of disease transmission. *Math. Biosci.* **2002**, *180*, 29–48. [[CrossRef](#)]
31. Mitchell, C.; Kribs, C. A comparison of methods for calculating the basic reproductive number for periodic epidemic systems. *Bull. Math. Biol.* **2017**, *79*, 1846–1869. [[CrossRef](#)] [[PubMed](#)]
32. Zhang, F.; Zhao, X.Q. A periodic epidemic model in a patchy environment. *J. Math. Anal. Appl.* **2007**, *325*, 496–516. [[CrossRef](#)]
33. Tian, J.P.; Wang, J. Some results in Floquet theory, with application to periodic epidemic models. *Appl. Anal.* **2015**, *94*, 1128–1152. [[CrossRef](#)]
34. Smith, H.L.; Waltman, P. *The Theory of the Chemostat: Dynamics of Microbial Competition*; Cambridge University Press: Cambridge, UK, 1995.
35. Zhao, X.Q. *Dynamical Systems in Population Biology*; Springer: Berlin/Heidelberg, Germany, 2003.
36. World Bank. Birth Rate, Crude. Available online: <https://data.worldbank.org/indicator/SP.DYN.CBRT.IN> (accessed on 1 June 2023).
37. World Bank. Mortality Rate, Infant. Available online: <https://data.worldbank.org/indicator/SP.DYN.IMRT.IN> (accessed on 1 June 2023).
38. Wain, J.; Diep, T.S.; Ho, V.A.; Walsh, A.M.; Hoa, N.T.T.; Parry, C.M.; White, N.J. Quantitation of bacteria in blood of typhoid fever patients and relationship between counts and clinical features, transmissibility, and antibiotic resistance. *J. Clin. Microbiol.* **1998**, *36*, 1683–1687. [[CrossRef](#)] [[PubMed](#)]
39. Crump, J.A.; Luby, S.P.; Mintz, E.D. The global burden of typhoid fever. *Bull. World Health Organ.* **2004**, *82*, 346–353. [[PubMed](#)]
40. Fatima, M.; Kumar, S.; Hussain, M.; Memon, N.M.; Vighio, A.; Syed, M.A.; Chaudhry, A.; Hussain, Z.; Baig, Z.I.; Baig, M.A.; et al. Morbidity and mortality associated with typhoid fever among hospitalized patients in Hyderabad district, Pakistan, 2017–2018: retrospective record review. *JMIR Public Health Surveill.* **2021**, *7*, e27268. [[CrossRef](#)] [[PubMed](#)]
41. Cho, J.C.; Kim, S.J. Viable, but non-culturable, state of a green fluorescence protein-tagged environmental isolate of *Salmonella typhi* in groundwater and pond water. *FEMS Microbiol. Lett.* **1999**, *170*, 257–264. [[CrossRef](#)]

42. Saltelli, A. Sensitivity analysis for importance assessment. *Risk Anal.* **2002**, *22*, 579–590. [[CrossRef](#)]
43. Arriola, L.; Hyman, J.M. Sensitivity analysis for uncertainty quantification in mathematical models. In *Mathematical and Statistical Estimation Approaches in Epidemiology*; Springer: Dordrecht, The Netherlands, 2009; pp. 195–247.
44. Marino, S.; Hogue, I.B.; Ray, C.J.; Kirschner, D.E. A methodology for performing global uncertainty and sensitivity analysis in systems biology. *J. Theor. Biol.* **2008**, *254*, 178–196. [[CrossRef](#)] [[PubMed](#)]
45. Saltelli, A.; Tarantola, S.; Chan, K.S. A quantitative model-independent method for global sensitivity analysis of model output. *Technometrics* **1999**, *41*, 39–56. [[CrossRef](#)]
46. Bacaër, N. Approximation of the basic reproduction number R_0 for vector-borne diseases with a periodic vector population. *Bull. Math. Biol.* **2007**, *69*, 1067–1091. [[CrossRef](#)]

Disclaimer/Publisher’s Note: The statements, opinions and data contained in all publications are solely those of the individual author(s) and contributor(s) and not of MDPI and/or the editor(s). MDPI and/or the editor(s) disclaim responsibility for any injury to people or property resulting from any ideas, methods, instructions or products referred to in the content.